NIST Technical Note
NIST TN 2316

Pre-conceptual Design Activities of the NIST Neutron Source

Preliminary Neutronics Assessments

Osman Ş. Çelikten
Abdullah G. Weiss
Dağıstan Şahin

This publication is available free of charge from:
https://doi.org/10.6028/NIST.TN.2316

NIST NATIONAL INSTITUTE OF STANDARDS AND TECHNOLOGY
U.S. DEPARTMENT OF COMMERCE

NIST Technical Note
NIST TN 2316

Pre-conceptual Design Activities of the NIST Neutron Source

Preliminary Neutronics Assessments

Osman Ş. Çelikten
Abdullah G. Weiss
Dağıstan Şahin
Reactor Operations and Engineering
NIST Center for Neutron Research

This publication is available free of charge from:
https://doi.org/10.6028/NIST.TN.2316

November 2024

U.S. Department of Commerce
Gina M. Raimondo, Secretary

National Institute of Standards and Technology
Laurie E. Locascio, NIST Director and Under Secretary of Commerce for Standards and Technology

NIST TN 2316
November 2024

Certain commercial equipment, instruments, software, or materials, commercial or non-commercial, are identified in this paper in order to specify the experimental procedure adequately. Such identification does not imply recommendation or endorsement of any product or service by NIST, nor does it imply that the materials or equipment identified are necessarily the best available for the purpose.

NIST Technical Series Policies
Copyright, Use, and Licensing Statements
NIST Technical Series Publication Identifier Syntax

Publication History
Approved by the NIST Editorial Review Board on 2024-11-25

How to Cite this NIST Technical Series Publication
Çelikten OŞ, Weiss AG, Şahin D, (2023) Pre-conceptual Design Activities of the NIST Neutron Source: Preliminary Neutronics Assessments. (National Institute of Standards and Technology, Gaithersburg, MD), NIST Technical Note (TN) NIST TN 2316. https://doi.org/10.6028/NIST.TN.2316

NIST Author ORCID IDs
Osman Ş. Çelikten: 0000-0002-4499-8699
Dağistan Şahin: 0000-0002-5256-1809
Abdullah G. Weiss: 0000-0003-1134-1735

Contact Information
osman.celikten@nist.gov
abdullah.weiss@nist.gov
dagistan.sahin@nist.gov

Submit Comments
abdullah.weiss@nist.gov
100 Bureau Dr, MS 6101, Gaithersburg, MD, 20899, USA

Abstract

The NIST Center for Neutron Research (NCNR) hosts the National Bureau of Standards Reactor (NBSR), which has been operational since 1967. The NBSR is an aging reactor, and current NCNR facilities could not keep up with ever-increasing scientific demand with the emergence of increasing technological and scientific developments. Therefore, NIST is pursuing a replacement reactor: the NIST Neutron Source, or NNS. The NNS is proposed to be a 20 Megawatt thermal (MW_{th}) compact-core-reactor, cooled and moderated by light water (H_2O). The core is fueled by nine high-assay low-enriched uranium-molybdenum (U-10Mo) monolithic curved plate fuel assemblies in a three-row by three-column square lattice. The NNS core is encased in a chimney surrounded by a heavy water (D_2O) filled reflector tank where two liquid deuterium (LD_2) cold neutron sources lie. This work discusses the neutronics of the NNS's pre-conceptual equilibrium core design, which includes its safety aspects. Descriptions of the design targets and anticipated reactor materials to be used are included along with the Monte Carlo N-Particle® (MCNP) model setup. A list of assumptions and model development details are shown to clearly illustrate the limitations of the analyses in this work. The equilibrium core computation process is shown alongside the converged fuel management scheme, which predicts a cycle length of 40 days with three fresh fuel assemblies each cycle. Neutron flux distributions illustrate the high leakage of thermal neutrons out of the core, which is desirable. Two critical parameters describe reactor utilization and fuel performance: the maximum power density and the maximum local integral fission density, or in short, fission density. For the NNS, the maximum power density is estimated to be 18 kW/cm^3, and the maximum local fission density is about 4.5×10^{21} $fissions/cm^3$. The same parameters are 4.88 kW/cm^3 and 2.0×10^{21} $fissions/cm^3$ for the NBSR. Note that the NBSR utilizes high-enriched U_3O_8 fuel and plans to use low-enriched U-10Mo fuel that is currently undergoing fuel qualification and demonstration testing at conditions relevant for NBSR and other U.S. high-performance research reactors by 2030. For comparison, the maximum power density and the maximum local fission density values for the NBSR utilizing U-10Mo fuel are estimated at 12.6 kW/cm^3 and 6.2×10^{21} $fissions/cm^3$, respectively, in fuel plates that are designed for a moderately thicker geometry than those planned for the NNS. Criticality safety assessments demonstrate negative reactivity coefficients for the moderator temperature, void, and H_2O to D_2O mixing from accidents involving the reflector tank. This technical note demonstrates that the current pre-conceptual NNS design is feasible and safe from a neutronics perspective.

Keywords

Criticality; NBSR; NCNR; Neutronics; NNS; Nuclear; MCNP; Safety.

Table of Contents

List of Tables

List of Figures

Acknowledgments

The authors acknowledge the team of individuals working on the design, including current members from the NCNR, active contributors outside the NCNR, and past contributors. Their names are listed below in alphabetical order.

Current NCNR Members

Osman Ş. Çelikten, Jeremy C. Cook, David J. Diamond, Noura R. Elsalamouny, Anil Gurgen, John M. Jurns, Hubert E. King, Charles F. Majkrzak, Thomas H. Newton, Dağıstan Şahin, Joy S. Shen, Abdullah G. Weiss

Active Contributors

Argonne National Laboratory, Nuclear Science and Engineering Division

Zhiee J. Ooi, John A. Stillman, Erik H. Wilson, Dhongik S. Yoon, Zhaopeng Zhong

Brookhaven National Laboratory, Nuclear Science and Technology Department

Lap-Yan Cheng, Arantxa Cuadra, Peter Kohut, Cihang Lu, Athi Varuttamaseni

Shimon Peres Negev Nuclear Research Center

Idan R. Baroukh, Eliezer Nahmani, Yaniv Shaposhnik

NIST, Engineering Laboratory, Structures Group

DongHun Yeo

Past Contributors

Danyal Turkoglu *(currently affiliated with USNC-Tech)*

Robert E. Williams

Zeyun Wu *(currently affiliated with Virginia Commonwealth University)*

Interns

Duncan Beauch, Evan Bures, Amir Dajani, Patrick Park, Eric Swanson, Breken Wallar

1. Introduction

The NIST Neutron Source (NNS) as proposed is a pool-type, water cooled and compact reactor design with 20 MW thermal power. The primary circuit components' layout is given in

Figure **1.**. The reactor core is composed of nine fuel assemblies which are cooled by light water that is separated by a chimney, designed to be of Zircalo-4, from the surrounding heavy water reflector tank housing two cold neutron sources, as shown in Figure 2. The NNS is planned to replace the National Bureau of Standards Reactor (NBSR), which is the current test reactor at NIST. The NBSR is primarily use as a neutron source for out-of-core neutron scattering and irradiation research. Two independent shutdown systems can secure the NNS as necessary: the safety blades and the reflector dump system. The primary shutdown system works by inserting the safety blades, and it can safely secure the reactor with the four safety blades positioned inside the reactor core. The reflector dump system provides a secondary shutdown mechanism where the heavy water (D_2O) in the reflector vessel is partially dumped to shut down the reactor.

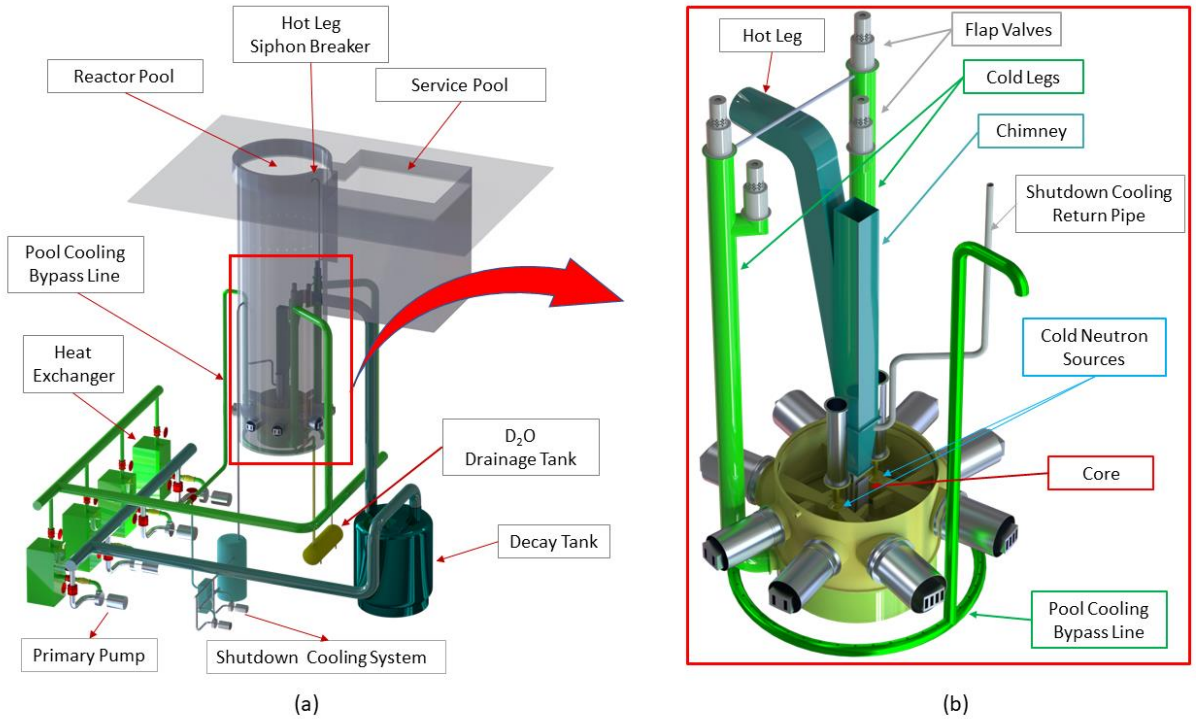

Figure 1. (a) 3D view of the main primary components, and (b) detailed view of zoomed in part in primary components.

This report describes the neutronic analysis of the NNS core and its reflector tank in terms of the nuclear criticality safety aspects. The widely accepted Monte Carlo N-Particle (MCNP) version 6.2 code package with cross-section data from ENDF/B-VII.1 and ENDF/B-VIII.0 libraries were used to complete neutronics analyses of the NNS core [1]. MCNP is a stochastic radiation transport modeling tool that is well-validated [2] and well-utilized as a core modeling tool and as a benchmark for other codes [3]. MCNP is accepted by the United States Nuclear Regulatory Commission (NRC) for safety and core modeling neutronics predictions [4]. For this work, the

MCNP model is used to assess the core neutronic characteristics; fuel cycles and burnup evolution; neutron flux distributions throughout the core; fuel assembly power and integral fission density distributions; and reactivity control in the core. Integral fission density is the total number of fissions occurred per volume of fuel—it is called fission density in this report. Relevant technical terms and definitions used in this report are provided in Table 1.

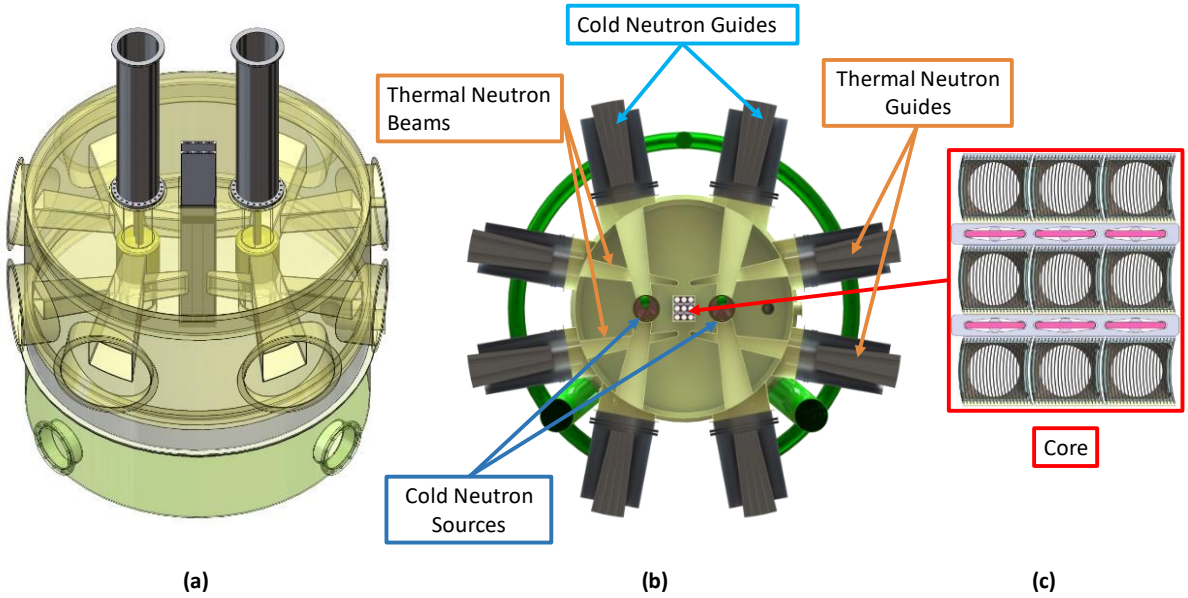

Figure 2. (a) 3D frontal view of reflector tank and support structures, (b) top view of reflector tank, and (c) top view of the core.

Table 1. Definitions for keywords in this document.

Keyword	Definition
Beginning of Cycle (BOC)	The BOC is the full power operation point at 1.5 days after the cycle startup. The *BOC period* covers the 8.5 days following the SU period. (see "cycle, cycle state" definition)
Cold Neutrons	Neutrons with energies below ~5 meV. The wave-particle duality of the neutron allows this range to be described by neutron wavelengths greater than ~0.4 nm.
Cold Neutron Source (CNS)	Cold neutron generation typically requires a dedicated Cold Neutron Source (CNS). The CNS consists of a chamber with a cryogenically cooled moderator placed in or near the peak of the unperturbed thermal neutron flux.

Keyword	Definition
Control Blade	Vertically driven neutron-absorbing plates are used to adjust core reactivity. Two control blades are used to separate the three fuel assemblies in the central/inner column of the core (Figure 2 (c)).
Cycle, Cycle State	A reactor cycle is the duration of time when the reactor is at power, i.e., critical. The reactor cycle can be divided into multiple cycle states for detailed analysis. The period of these cycle states, which include the following, are defined as a part of a reactor cycle. Their visual description is presented in Figure 3. - Startup (SU) period - Beginning of Cycle (BOC) period - 2nd Quarter of Cycle (Q2) period - Middle of Cycle (MOC) period - 4th Quarter of Cycle (Q4) period - End of Cycle (EOC) period
Core Loading	The pre-determined arrangement of fuel assemblies for reactor operations.
End of Cycle (EOC)	The EOC is the end of an operating cycle, where the reactor is shut down for reactor maintenance. The *EOC period* is the final part of a cycle, which covers eight days representing the anticipated maintenance period of the reactor prior to the next operational cycle.
Effective Multiplication Factor (k_{eff})	k_{eff} is a dimensionless number which equals the number of neutrons produced within the current generation divided by the neutrons lost in the preceding generation. A value of unity implies a critical reactor where the fission chain reaction can be sustained.
Fission Density	Integral fission density, or fission density, is the total number of fissions per unit volume of fuel.
Fuel	Material containing fissionable or fissile material, such as ^{235}U. This work adopts high-assay low-enriched U-10Mo foil as fuel.
Fuel Plate (FP)	A product which contains a fuel foil (thin sheet of U-10Mo alloy with zirconium interlayer) encapsulated and bonded within aluminum alloy cladding.
Fuel Assembly (FA)	A mechanical assembly comprised of fuel plates and non-fueled hardware.

Keyword	Definition
Integral Worth	The integral worth ($\Delta\rho$) of a control-blade is the total amount of positive reactivity that is yielded from the withdrawal of a safety or control blade from their inserted position.
Middle of Cycle (MOC)	The MOC is the full power operation point in the middle of an operating cycle. The *MOC period* covers the third one-quarter part of an operating cycle.
Power Peaking Factor	The power peaking factor is a metric that measures the power density in a certain location such as a fuel plate or a fuel assembly or an axial part of the fuel/assembly section relative to the average power density in the reactor core .
Quarter 2 (Q2)	The full power operation time corresponds to the end of the -BOC period of an operating cycle. This *Q2 cycle period* covers the second quarter of the operating cycle (the 10 days following the Q2 cycle state).
Quarter 4 (Q4)	The full power operation time corresponds to the end of the MOC period of an operating cycle. The *Q4 period* covers the last quarter of an operating cycle.
Reactivity (ρ)	Deviation of the k_{eff} from unity, or $(k_{eff}-1)/k_{eff}$. Positive reactivity insertion tends to increase the reactor power , while negative reactivity insertion tends to decrease the reactor power.
Excess Reactivity	Total reactivity stored in a critical core configuration. Excess reactivity is calculated with the complete withdrawal of all control and safety blades from the reactor core.
Reactor Core	The control and safety blades, and an arrangement of multiple fuel assemblies in a pre-determined configuration.
Safety Blade	Vertically driven neutron-absorbing plates are used to shutdown the chain reaction. Four safety blades separate each pair of fuel assemblies in the outer columns of the core (Figure 2(c)).
Shutdown System	Mechanical systems that could introduce sufficient negative reactivity to shut down the reactor, which include the safety blades and the reflector dump systems.
Startup (SU)	The startup (SU) state is the first point of full power operation in a cycle. The *SU period* covers the first 1.5 days of operation in the cycle. It allows the model to account for the effects of short-term buildup of some parasitic isotopes such as xenon to equilibrium concentration.

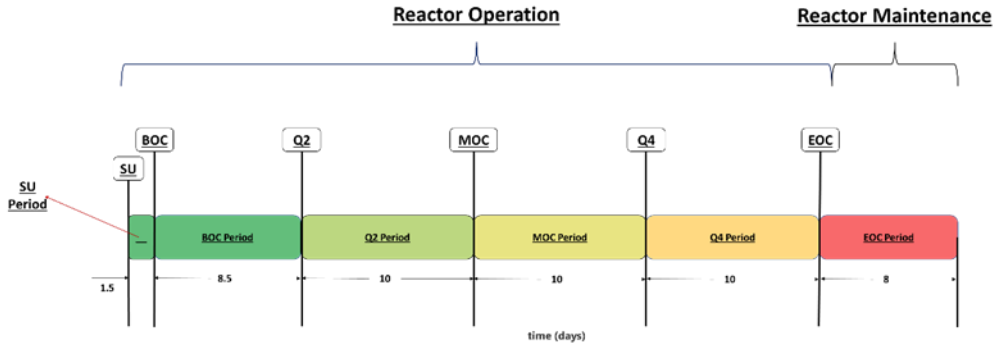

Figure 3. Illustration of the Cycle and the Cycle State

1.1. Design Targets

The design of the NNS core is a meticulous and multifaceted process that revolves around achieving specific performance goals and ensuring the safety and efficiency of the system. The primary design targets of the NNS core encompass a delicate balance among generating a reliable and abundant supply of neutrons for the experiments to serve as versatile tools for a wide range of scientific investigations, ensuring operational flexibility to accommodate diverse research needs, and incorporating safety features to protect the personnel, the public, and the environment. The design process considers factors such as fuel cycle sustainability, nuclear proliferation resistance, and adherence to regulatory standards. By addressing these design targets, the NNS can play a crucial role in providing a secure neutron source for the scientific community in the future. To that end, a list of preliminary design targets that were met to maintain the safe operation of the NNS is presented in Table 2. The table contains each target and their explanation of the corresponding basis/reasoning.

Table 2. A list of the design targets for the NNS.

Target	Basis
Nominal thermal power is maintained at 20 MW.	The 20 MW power level is to reinforce the NCNR's operational expertise, which spans over 50 years on the NIST campus. Other power levels may be considered based on cold neutron source performance.
Safety blades insert sufficient reactivity at any cycle state to shut down the core, even with one blade stuck (malfunctioning).	Conformity with regulatory requirements of the stuck-blade criterion, as defined in NUREG-1537 [5]. In particular, the remaining safety blades, excluding the stuck-blade, must insert sufficient negative reactivity to safely shut down the core from the reference core condition to greater than or equal to the specified minimum shutdown margin.
The reflector dump system inserts sufficient reactivity to shut down the core at any cycle state (excluding the safety blades).	Demonstrate the effectiveness of the reflector dump shutdown system and enable a backup safety shutdown system.

Target	Basis
The moderator exhibits a negative reactivity feedback coefficient at all operating conditions.	Ensure that an increase in moderator temperature is not leading to positive reactivity addition to the system.
The cycle length is ~40 days.	Maintain similar operating schedules to the NBSR. Longer cycle lengths may be considered in the future.
The core excess reactivity must be kept as low as practical.	To be consistent with the cycle duration requirements, and the need to compensate xenon, as well as reactivity changes due to possible future irradiation facilities.
The rate of reactivity insertion by control blades would be controlled via the blade removal speed.	To prevent reactivity accidents, reduce thermal and mechanical stresses on reactor components, and ensure that operators have adequate time to manage reactor conditions effectively.
Sufficient cooling capacity exists to prevent fuel overheating and loss of integrity for all anticipated reactor operating conditions	To ensure the safety and integrity of the system, and to ensure compliance with regulatory standards and technical recommendations.

1.2. Reactor Materials

The NNS, as proposed, is a compact core to maximize neutron leakage for out-of-core neutron scattering and irradiation research. The core and its peripheral structure's materials were selected by considering desirable neutronics characteristics, thermal-hydraulics behavior, and structural stability. This section describes the materials used in the core and its peripheral components to accomplish the design targets and sustain the neutron economy along the NNS's operational cycle.

The NNS uses high-assay low-enriched U-10Mo (uranium with 10 % molybdenum by weight) monolithic fuel, which contains ~19.75 weight percent enriched uranium. The fuel is in plate-type assemblies similar to the ones utilized in existing high-performance research and test reactors in the US, such as the NBSR, High Flux Isotope Reactor, and the Advanced Test Reactor. A single fresh FP contains 34.7 g of U-235. The total equilibrium core loading contains approximately 32.2 kg of uranium and 92 g of plutonium at SU. Each FP contains the U-10Mo fuel bounded by two thin zirconium interlayers preventing unwanted fuel-clad interactions with the aluminum alloy-6061 (Al-6061) cladding [6, 7]. The low absorption cross-section and radiation damage durability of zirconium alloys (such as Zircaloy) make them suitable for usage in the core's structural components and peripherals such as beam tubes and cold neutron sources.

The control and safety blades in the NNS have the same geometry and are composed of hafnium as a poison material. Hafnium offers increased longevity and reduced maintenance demands when compared to cadmium, which is the control blade material used in the NBSR. Cadmium (Cd) burnable poison wires are located inside of the Al-6061 side plates that keep the FPs together, but the location of the Cd wires is slightly shifted toward the lower part of the side plates to suppress the high power peaking of fresh FAs around the bottom central region of the reactor.

2. Analysis Methodology and Modeling Assumptions

The core is composed of nine FAs, each with 21 curved FPs. Images of the three-dimensional (3D) MCNP model of the reactor and core are shown in Figure 4 through Figure 6. The MCNP model of the NNS is developed under the assumptions listed in Table 3, which are categorized as either geometric, materials, or power assumptions. One of the most important design considerations is that U.S. civilian research and test reactors are planned to use LEU fuels produced by down-blending high-enriched uranium (HEU). Y-12 National Security Complex is planned to produce the LEU fuel as part of the Research Reactor Uranium Supply Program. The HEU contains a considerable amount of parasitic uranium isotopes, such as ^{232}U, ^{234}U, and ^{236}U, which are included in the modeling and analysis [8, 9].

Table 3. List of specifications and modeling assumptions for the MCNP model of the NNS.

Category	Assumption	Explanation
Geometric	Flat plates are modeled instead of curved plates.	This assumption is adopted for simplicity and has been found successful in the analysis of the NBSR [10]. Note that the same moderator-to-fuel ratio is maintained.
	Multiple structural components are neglected for simplicity.	The following components are absent from the models as they are considered to have negligible effects on the neutronics model: - Piping, including chimney - The bottom supports and upper shells for the cold neutron sources - Latches and legs of FAs - Inlet pipe openings in the lower plenum
Materials	Moderator temperature is assumed to be constant at 293 K.	The moderator temperatures are proposed to be 318 K (inlet) and 331 K (outlet) with an average of 324.5 K. The cross-section data for the moderator would not be much different with respect to the available 293 K data. S(α,β) data are used for the light water at a relevant temperature of 323 K and for the heavy water at 300 K.
Power	20.2 MW is simulated instead of 20 MW.	Some of the fission heat is deposited in external structures other than FAs and the moderator. An 0.2 MW of additional power ensures such losses are accounted for.

Besides the Y-12 fuel material, the following assumptions were made:

- The fuel core in each fuel plate is zoned laterally and axially to account for spatial variations in the fuel composition due to burnup. Axially, the fuel core is discretized into ten zones (Figure 7). Laterally, the fuel is discretized uniformly into three zones (Figure 8). Altogether thirty rectangular zones are used to describe the fuel where most of the fuel core is discretized into twenty-four larger zones while the top and bottom of the fuel core consist of six smaller zones.
- The Cd burnable absorber wires are axially discretized into five zones to allow for detailed tracking of the Cd depletion.
- Two cold neutron sources are located on the east and west (arbitrary east/west) sides of the reactor as shown in Figure 4 and Figure 6.
- Each CNS is in contact with two cold neutron beamlines.
- Each cold neutron beamline intersects a thermal beamline which is 23 cm by 9 cm, oval in shape, and located on the north and south sides of the reactor.
- Cold neutron beamlines have a conical geometry to enable more experimental locations and increase the cold neutron brightness in the beams.
- The narrowest window clearance of the cold neutron beams near the CNS is approximately 15 cm by 25 cm, and it expands along the cold neutron guide tube.
- The core region is surrounded by a cylindrical heavy water reflector tank that is 131 cm in outer and 130 cm inner radius. The tank is 134 cm in height and can keep up to 130 cm of the heavy water column in it, as shown in Figure 4 and Figure 6. The reflector tank serves to improve neutron economy and CNS brightness.
- It is assumed that the reflector tank temperature is kept constant by a separate cooling system.
- The cross-sections of all materials except for the CNSs are kept at room temperature (293 K).

A sample FA and FP are represented in the elevation (XZ) and planar (XY) planes in Figure 7 and Figure 8, respectively. A total of twenty-one FPs are present in each FA, where each plate contains U-10Mo fuel core encased in Al-6061 cladding. As mentioned, a thin zirconium interlayer separates the U-10Mo and Al-6061 to help prevent fuel-clad chemical interaction. Although the MCNP model does not contain this zirconium interlayer, it is expected to be approximately 8 μm thick in the conceptual design [6]; A zirconium interlayer of this thickness is not expected to have any effect on neutronic analysis results. Note that the fuel utilizes cadmium (Cd) wires as burnable poison to suppress the local power of fresh fuel within the operating cycle. Laterally, two Cd wires are placed on either side of the FP as shown in Figure 8(b). The Cd wires slide into H_2O-filled T-shaped slots within the side plates, where the water can provide some level of cooling for the Cd.

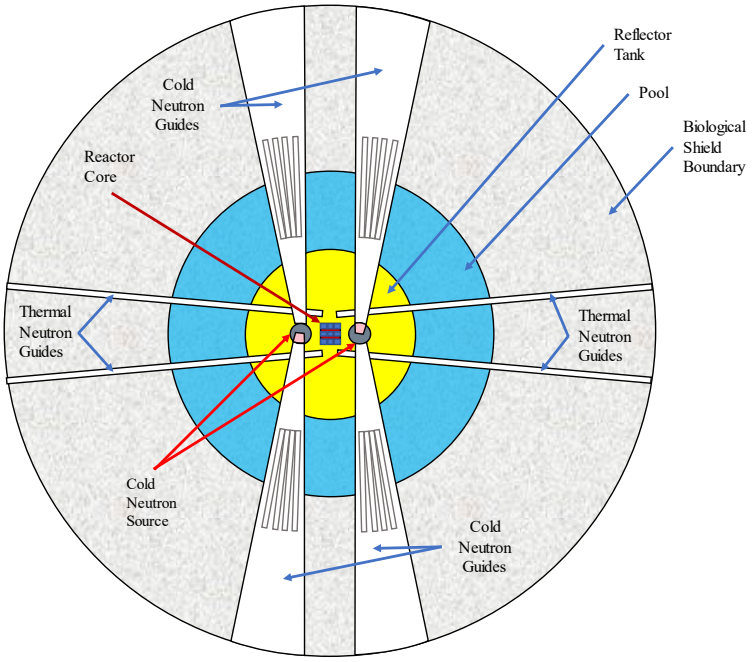

Figure 4. Planar (XY) view of the MCNP model.

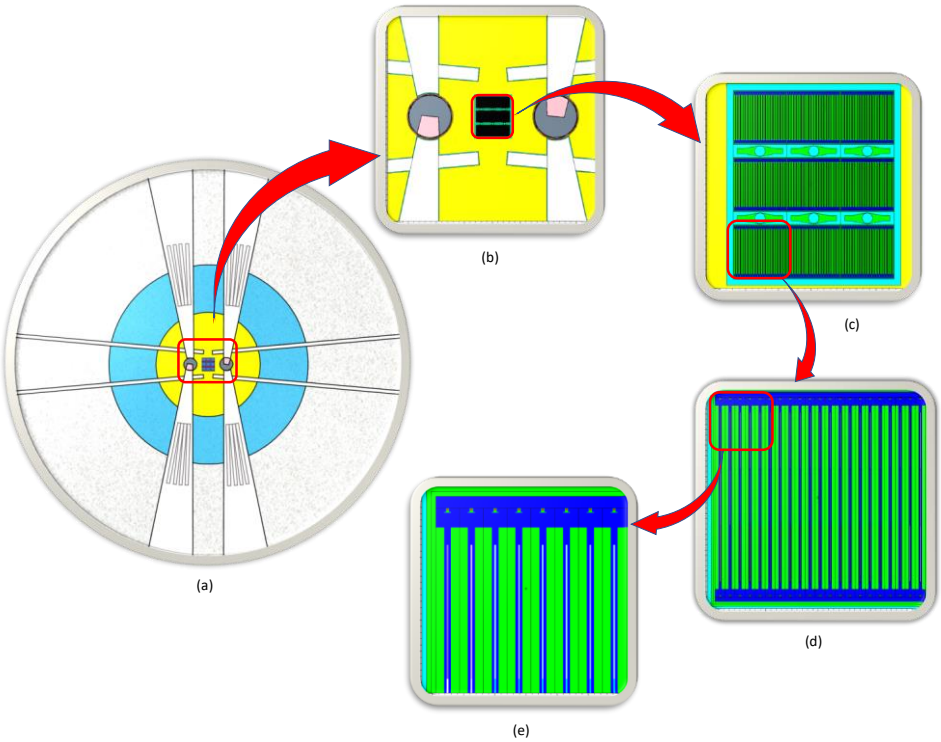

Figure 5. (a) Planar (XY) view of the MCNP model, (b) detailed view of the core with cold neutron sources, (c) the fuel assemblies and control/safety blades, (d) full view of a single fuel assembly, and (e) close-up view of cadmium burnable absorber wires and fuel.

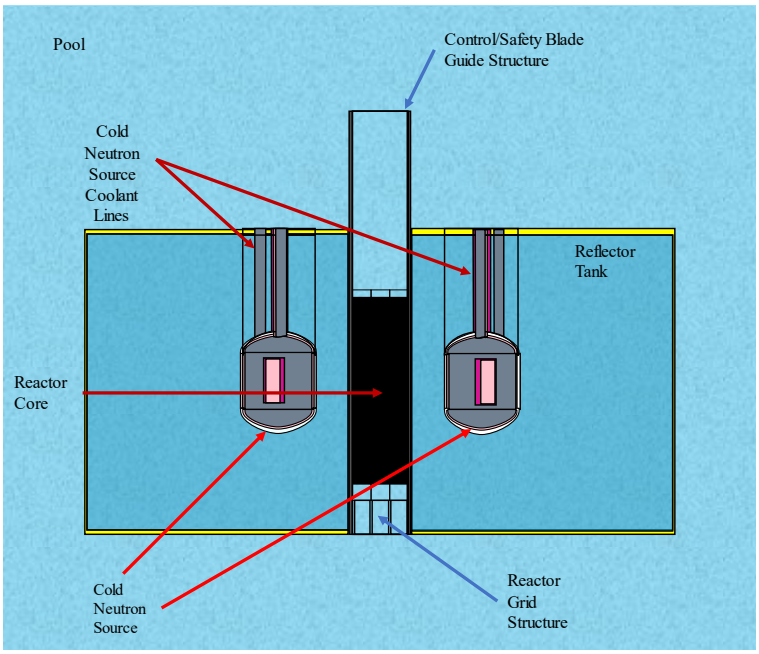

Figure 6. Elevation (XZ) view of the MCNP model.

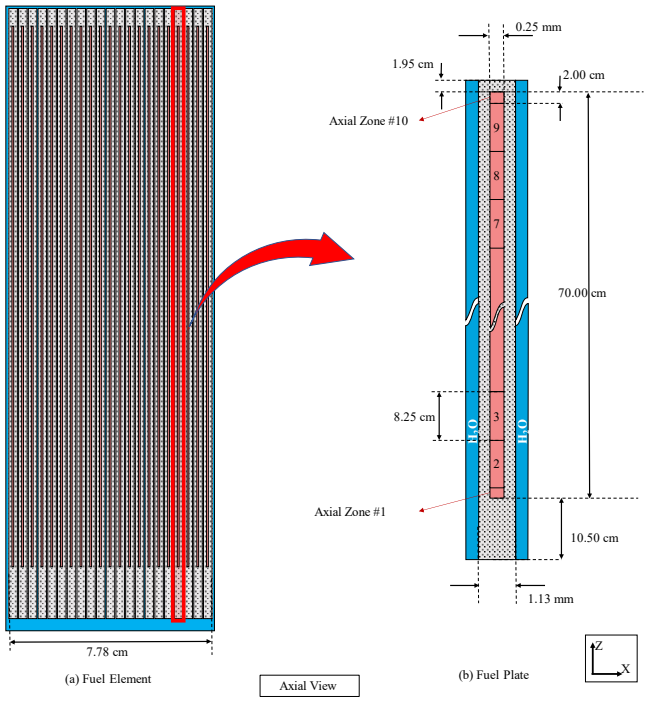

Figure 7. A detailed description of (a) an FA and (b) an FP in the elevation (XZ) plane[1]. View at Y=0.

[1] Note that this illustration is not to scale. All axial zones are 8.25 cm high except for zones 1 and 10, which are 2 cm high.

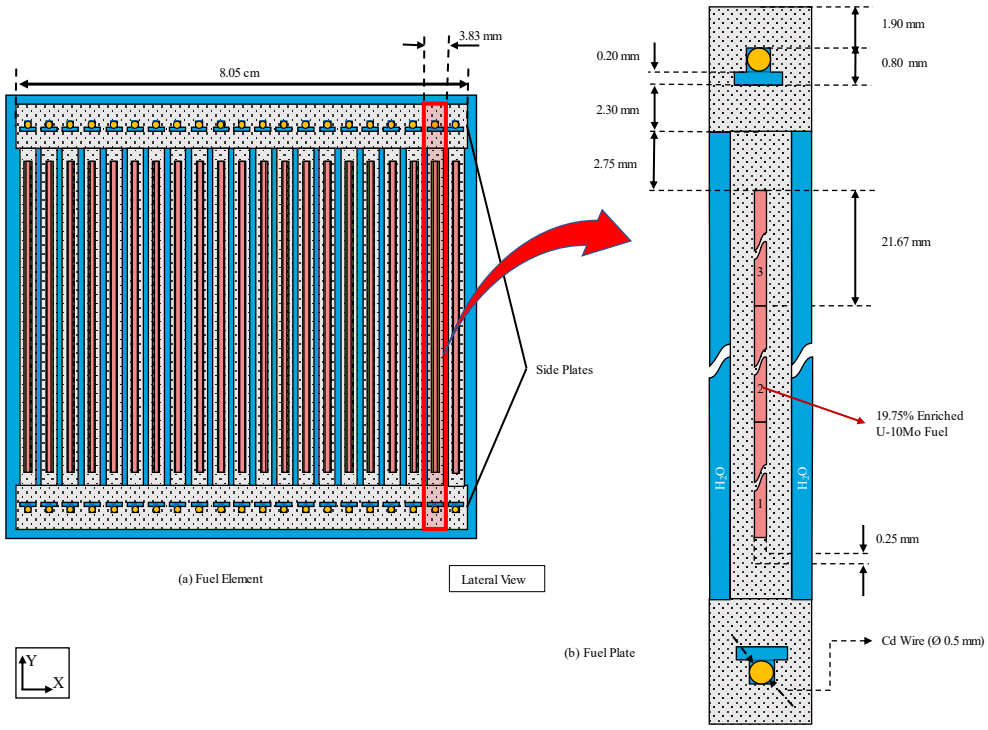

Figure 8. A detailed description of (a) an FA and (b) an FP and surrounding side plates in the planar (XY) plane[2]. View at Z=0.

2.1. Core Loading Pattern and Fuel Management Scheme

The NNS core has a simple fuel loading pattern since the core does not contain many FAs (see Figure 9). Only three new FAs are introduced at the beginning of each cycle. This loading pattern in the equilibrium core cycles is designed to allow simple refueling operation. The inner column of the core is loaded with three fresh FAs (identified as A12, B22, and C32, and in checkerboard green in Figure 9); which are moved to their second cycle locations in the following cycle (gridded yellow) and then to their third and final cycle positions (dotted red).

As shown in Figure 9, all assemblies follow a fuel identification that describes their initial and current locations in the core. The first letter of the fuel identification is the original row where it was loaded in its initial cycle. For instance, if a FA's initial location is row B, it will stay in row B throughout its operational life (all three cycles). However, if a FA begins in row A or C, it will alternate between rows A and C in its consecutive cycles.

The second indicator in the fuel identification is a single or double apostrophe used to define the assembly's age in the core (i.e., the number of cycles it has been in the core). A single apostrophe denotes that the assembly was irradiated for a single cycle (hence it is in its second cycle), while a double apostrophe denotes that the assembly is in its final cycle (it has been in the core for two cycles). The last indicator in the fuel identification consists of a pair of digits describing the row and column of the assembly's current location in the 3 by 3 matrix. For example, A'31 denotes a

[2] Note that this illustration is not to scale. The fuel core is represented in 3 radial zones with a width of 2.167 cm (Y-direction).

second-cycle assembly that was loaded first in row A but now has moved to the third row (row C) and first column (the assembly shown in yellow at the bottom-left corner in Figure 9). The fuel management scheme can be summarized as follows.

$$A12 \rightarrow A'31 \rightarrow A''13$$

$$B22 \rightarrow B'23 \rightarrow B''21$$

$$C32 \rightarrow C'11 \rightarrow C''33$$

Note that the assemblies would be moved to a spent fuel pool upon completing their third cycle, after which they would be disposed of from the facility.

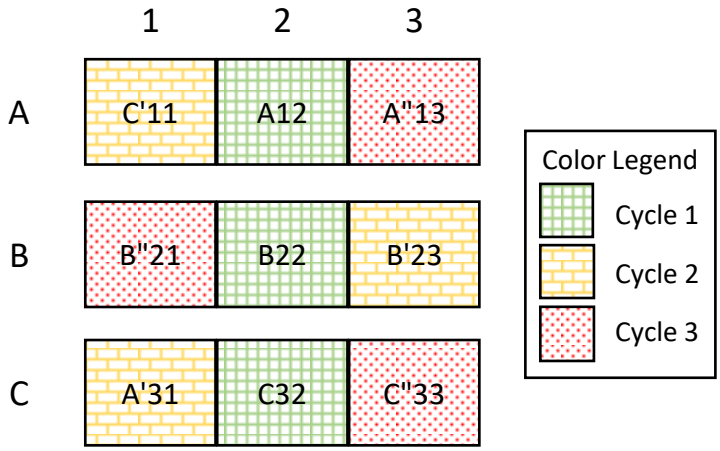

Figure 9. Fuel Management Scheme with fuel identifications shown on each FA location.

2.2. Equilibrium Core State

The equilibrium core state (ECS) is where fuel compositions, safety systems, and structures are at their nominal operating conditions. Nominal operation parameters andsafety analysis is limited to the equilibrium core state. The regulatory requirements must be met for all core states.. Figure 10 shows a flow chart to illustrate how the ECS search routine is conducted. The ECS routine starts with checking whether the current simulated cycle is the first cycle or not. In the first cycle, the entire core is loaded with fresh FAs with pre-determined compositions (currently, the initial loading of the startup core is not optimized), after which the compositions of those assemblies are used to step to the following cycles with the fuel management scheme presented in Figure 9. After the shuffling process or initial core loading, the control blade calibration module (shown on the bottom-left side of Figure 10) is started by the ECS routine to determine the blades' critical positions.

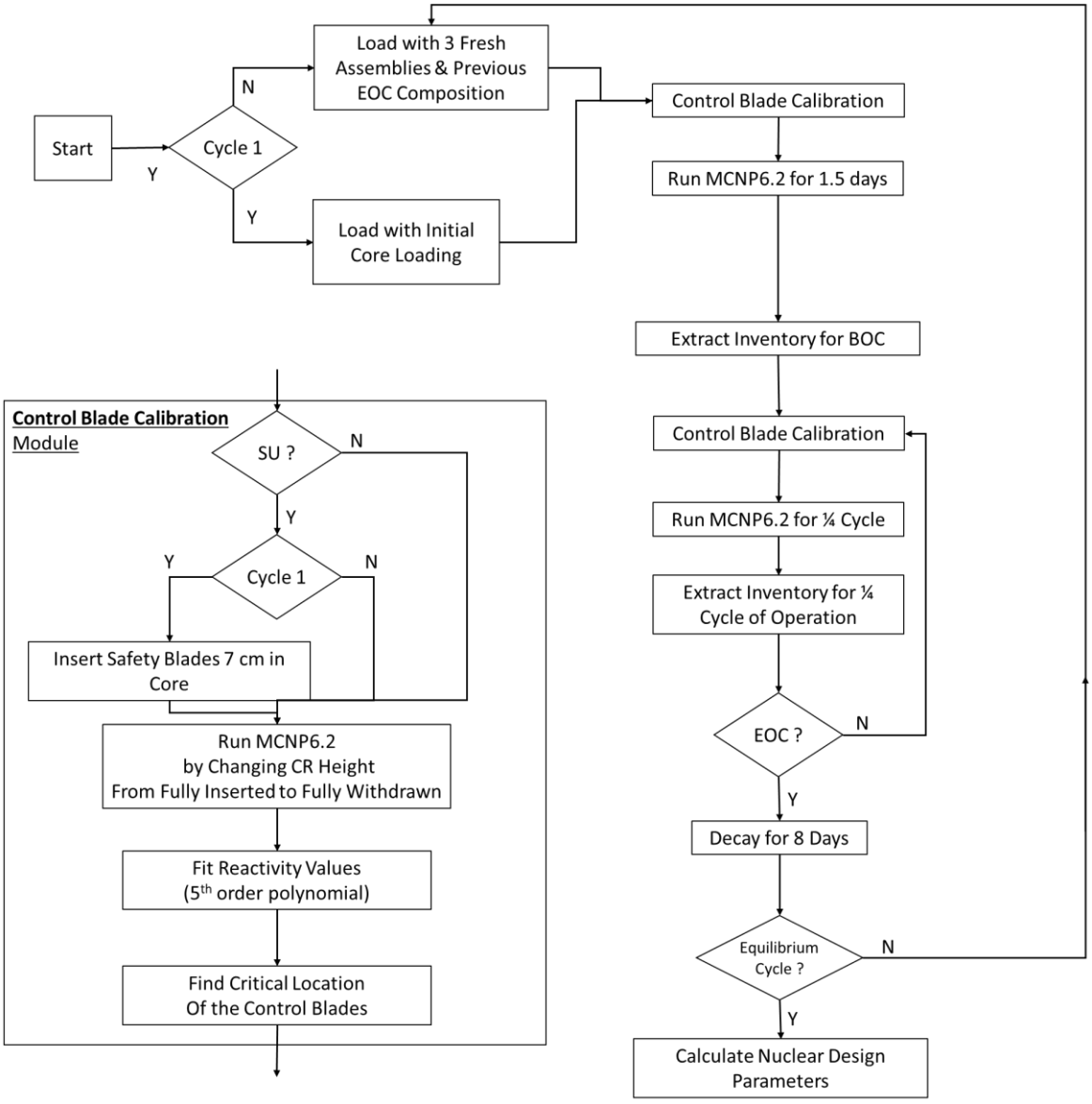

Figure 10. Logic flow chart of the approach to the equilibrium core state.

The control blade calibration module has been implemented as a generic module that covers all reactor core cycle states.

In all cycle states, MCNP simulations are run with control blades at heights ranging from the fully inserted position to the fully withdrawn position via the control blade calibration module while the safety blades are always fully withdrawn for the equilibrium cores, but are 7 cm inserted for the initial all-fresh core. This is done by 10 cm incrementally varying the blades' axial positions from fully inserted position to fully withdrawn position and tracking the resulting variation in the reactivity. The reactivity variation results of the system are then fitted to a 5^{th}-order polynomial as a function of the blades' location. The fitted 5^{th}-order polynomial function is used to estimate the critical positions of the control blades at a given cycle state. This is the same approach used for calibrating shim arms in the NBSR.

The reactor core cycle simulations start with a 1.5-day burnup simulation to represent the SU period that is used to observe the adverse effects of xenon accumulation inside the reactor core. Once the SU simulation is completed, required data are stored for future analyses. The SU output inventory and neutronics parameters (k_{eff} , average number of neutrons released per fission, control blade positions, etc.) are transferred to the BOC initial inventory where the control blade calibration module is run again before simulating the subsequent burnup run. This iterative procedure is repeated for each quarter of a cycle (Q2, MOC, Q4) until the end of the 40-day cycle is reached. When the 40-day cycle is reached at the EOC state, an eight-day decay simulation is performed to specifically track the short-lived active isotopes and Xe-135 content within the fuel in the typical maintenance period. Upon completion of this first cycle and any further cycles, the ECS routine checks if an equilibrium state has been reached, and then proceeds to extract the fuel compositions throughout the core.

The ECS routine utilizes multiple cycles to reach an equilibrium state. Equilibrium is assumed to be reached when excess reactivity is nearly unchanged (fluctuating within 150 pcm), at which point control blade positions are near unchanged (within 0.5 cm of the previous cycle's); and the material compositions in the FAs do not change much between subsequent cycles. The ECS routine then moves into the "Calculate Nuclear Design Parameters" mode. In this mode, the equilibrium core model is used to determine nuclear design parameters, such as neutron flux and power distributions, neutron spectra, control blades' reactivity worth, shutdown margins, and reactivity coefficients. The remainder of this report shows the core characteristics of the equilibrium NNS core.

3. Neutronic Design Characteristics of the NNS Core

3.1. Neutron Flux Distributions

The primary goal of the NNS is to provide neutrons to the experimental facilities, so it's important to understand the flux distribution throughout the core. Figure 11 is presented to understand the core and peripheral components and their location around the core. The neutron flux distributions throughout the core at the 3 cycle states SU, MOC, and EOC are presented four different energy groups in Figure 12 through Figure 15. Note that the neutrons are separated into four energy groups representing cold and thermal (less than 0.025 eV, Figure 12); epi-thermal (0.025 eV to 0.4 eV, Figure 13); resonance (0.4 eV to 100 keV, Figure 14); and fast groups (100 keV to 20 MeV, Figure 15). Cold neutron energies are usually assumed to be less than 0.005 eV, so the first energy group includes some thermal neutrons as well. The figures illustrate the spatial distribution of neutrons within the core for each of these groups at the SU, MOC, and EOC states for the ECS at 20 MW.

The cold and thermal neutron flux distribution is shown in Figure 12. As viewable in the figures, the cold neutrons with accompanying thermal neutronsis concentrated in the non-reentrance zones of the CNSs, which contains cryogenics moderator, as designed. The thermal flux profiles are represented in Figure 13. Since there is a high moderation ratio of D_2O in the reflector tank, it is consistently observed throughout all cycle states that the largest concentration of thermal neutrons is found near halfway between the CNSs and the core's edges. To direct thermal neutrons to the thermal beam tubes, the thermal beam tubes were positioned as close as possible to the reactor and in the area where the thermal flux is high. If the thermal beam tubes were placed at the top or bottom section of the reactor, they would be affected by changes in axial neutron density during the cycle due to the movement of the control blades. Since the central region of the reactor is less affected by the control blade movement during the cycle (in terms of neutron density), the thermal beam tubes intersect the cold beam tubes. Figure **14** and Figure 15 show that most of the resonance and fission (fast) neutrons reside in the core. Although such higher energy neutrons are not relevant to current planned instruments and research that NNS supports, they may be useful in the future if other experimental capabilities are deemed important for the NCNR.

The effectiveness of the reactor design and the CNS is demonstrated with the highest concentration of cold neutrons found in the CNS, while fast neutrons are almost exclusively within the fuel. Some insights can be drawn on how to better optimize the locations and orientations of the CNSs and the thermal neutron beams when analyzing these profiles. For example, the CNSs themselves perturb the cold neutron flux distributions. Such phenomena should be evaluated to further optimize the orientation of the CNSs and beams to maximize the cold neutrons flux delivered to scientific instrumentation.

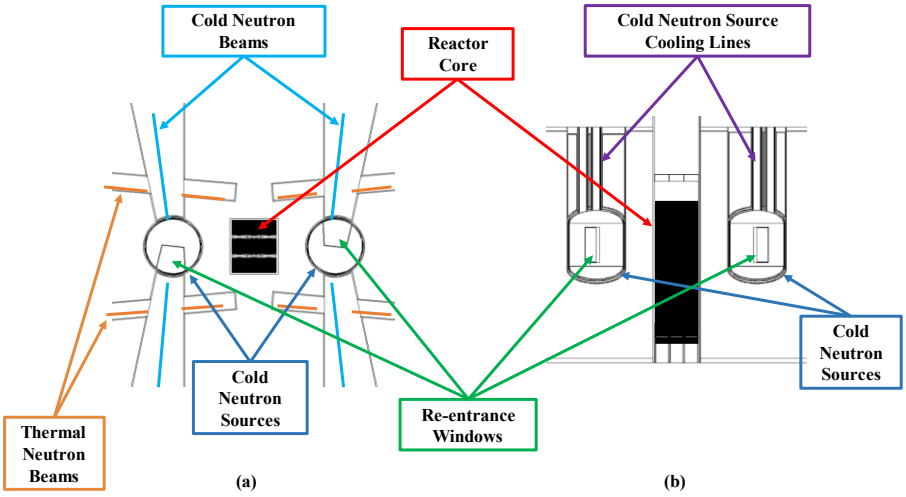

Figure 11. A representation of the core, CNSs, and their peripheral components in (a) the planar view (corresponds to Figure 4) and in (b) the elevation view (corresponds to Figure 6).

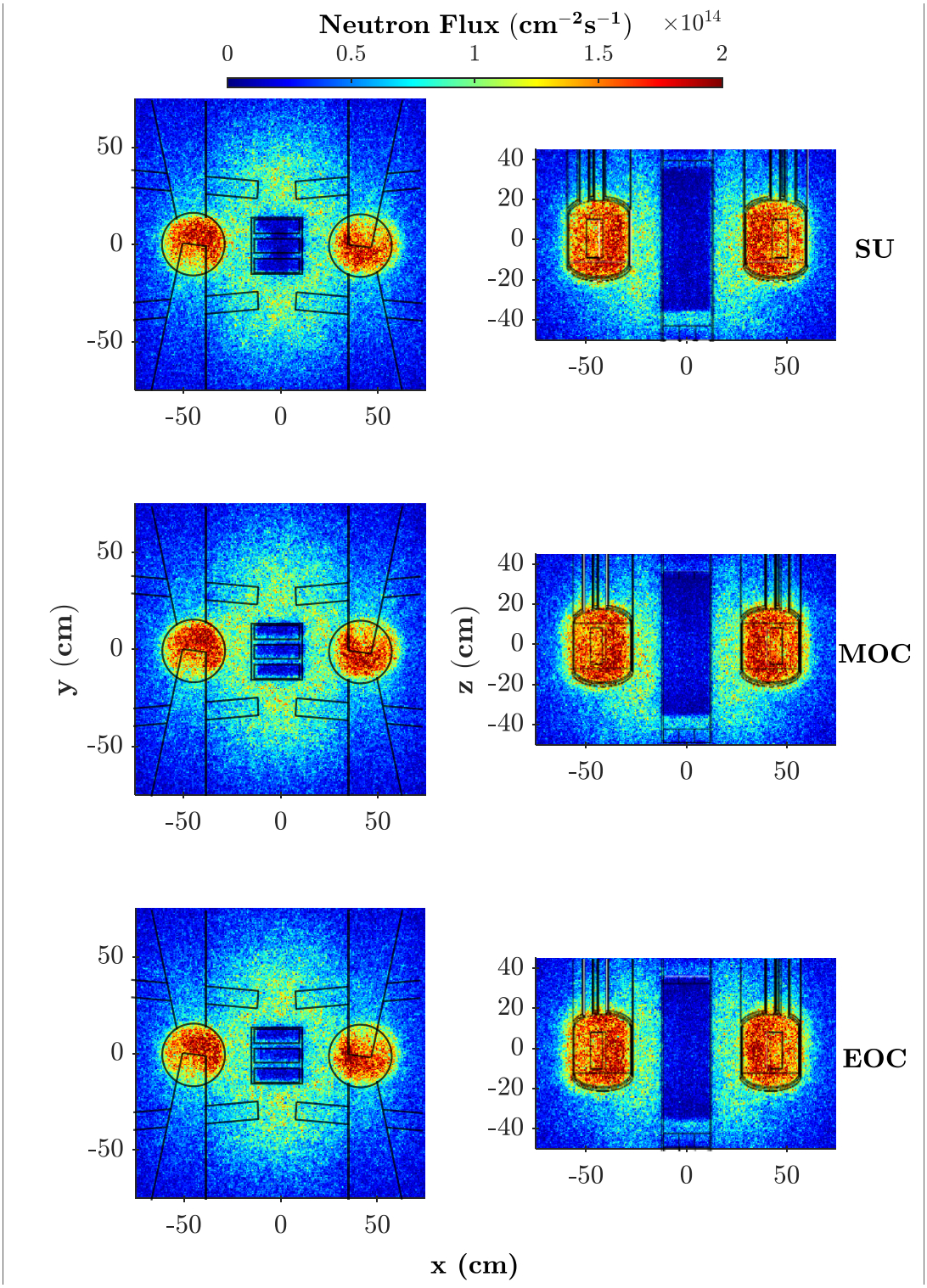

Figure 12. The cold and thermal neutrons (<0.025 eV) fluxes at SU, MOC, and EOC state[3].

[3] Note that both views are represented at their respective center planes, left views at the axial centerline (z=0), and right column views show a view at the radial centerline (y=0).

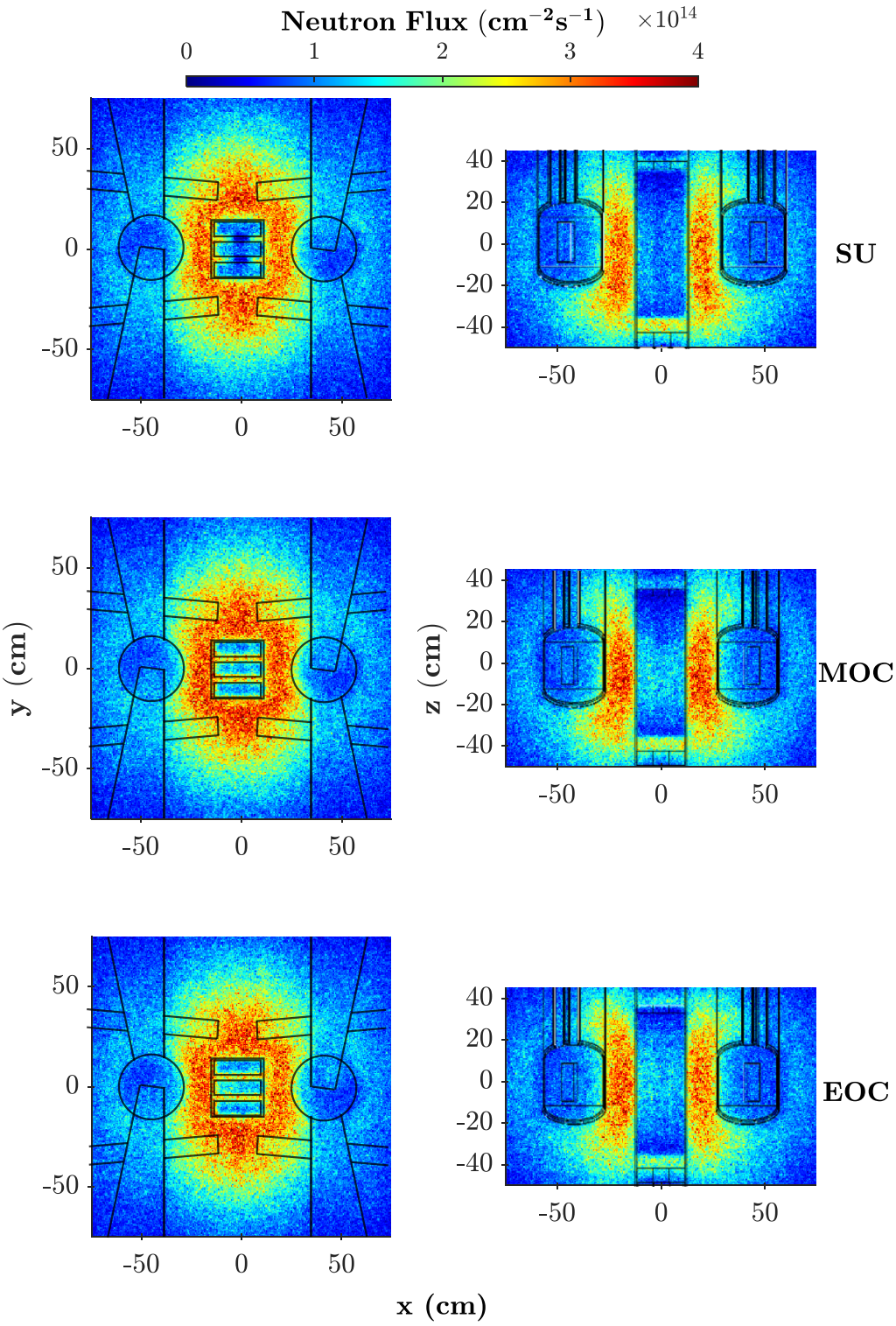

Figure 13. The epithermal neutron (0.025 eV to 0.4 eV) fluxesat SU, MOC, and EOC state[4].

[4] Note that both views are represented at their respective center planes, left views at the axial centerline (z=0) and right column views show a view at the radial centerline (y=0).

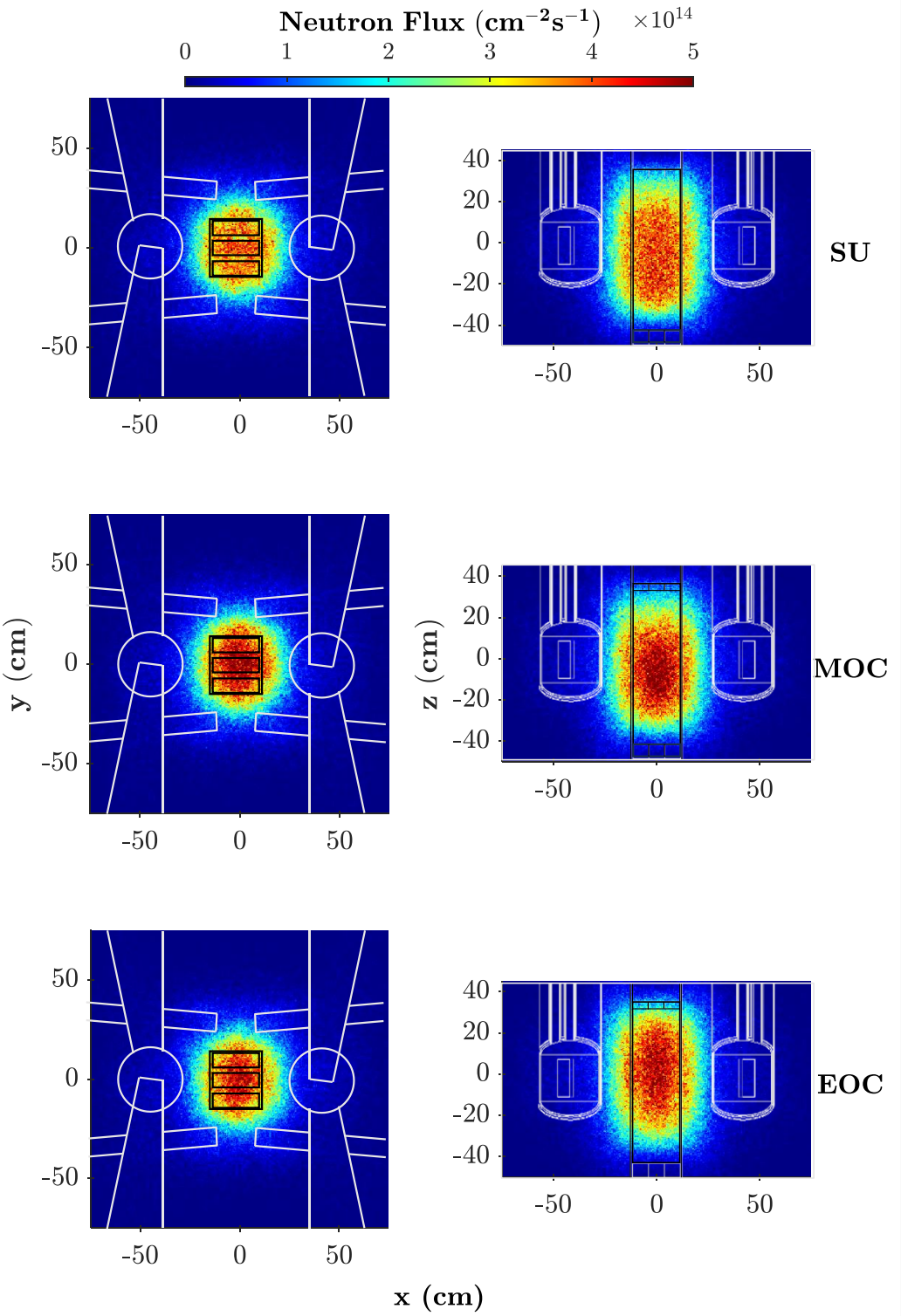

Figure 14. The resonance neutron (0.4 eV to 100 keV) flux profiles at SU, MOC, and EOC state[5].

[5] Note that both views are represented at their respective center planes, left views at the axial centerline (z=0), and right column views show a view at the radial centerline (y=0).

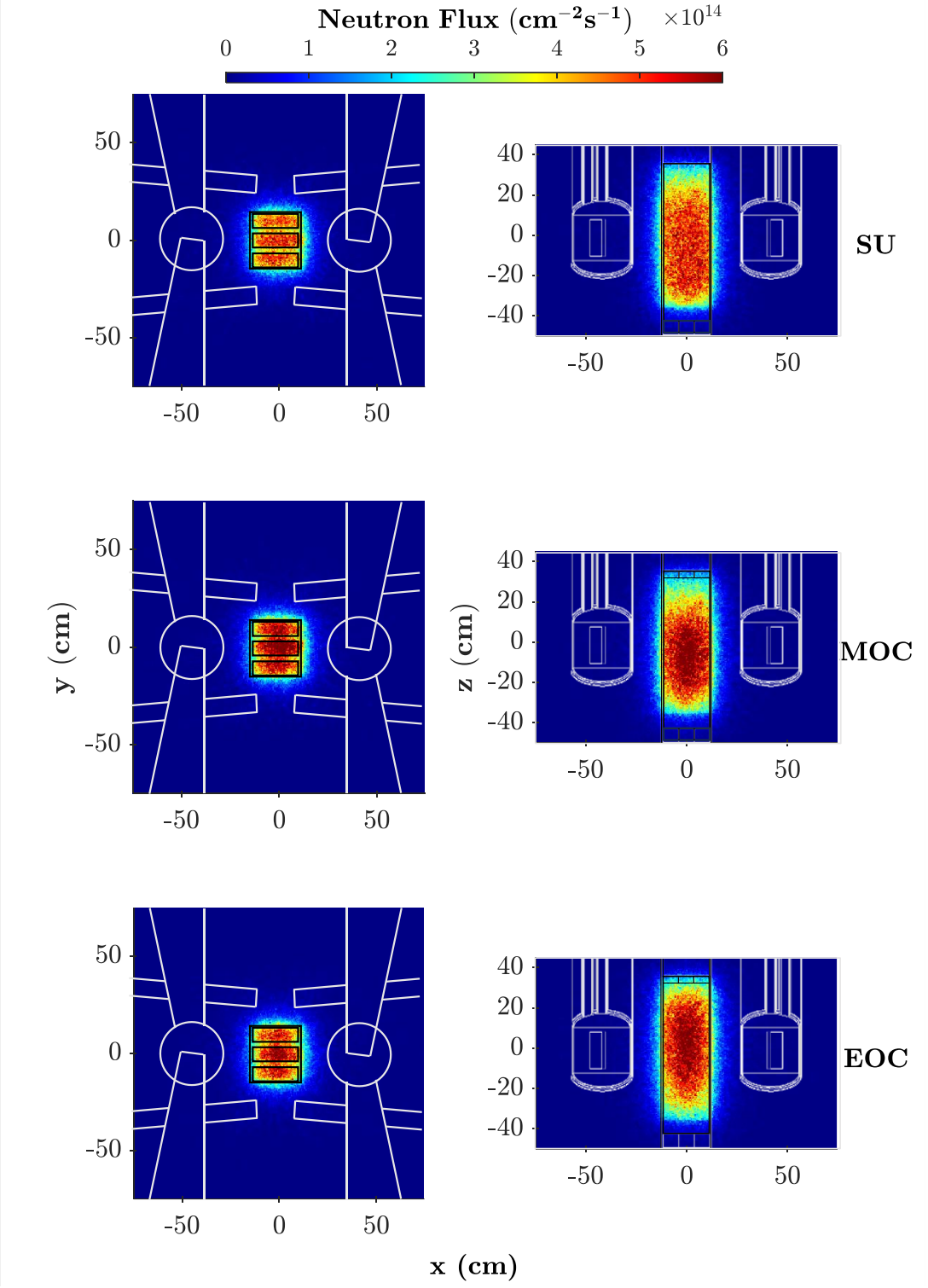

Figure 15. The fast neutron (100 keV to 20 MeV) flux profiles at SU, MOC, and EOC state[6].

[6] Note that both views are represented at their respective center planes, left views at the axial centerline (z=0), and right column views show a view at the radial centerline (y=0).

3.2. Power Distributions

By obtaining the power profiles inside the core region (such as lateral, axial, plate-wise, and transverse power distributions), the local hot-spot locations needed in the thermal-hydraulics and safety analyses can be determined. For that purpose, the power distributions are computed using fission energy deposition tallies in the MCNP model, where high spatial resolution is maintained by discretizing each FP into three transverse and 35 axial volumes (yielding 19,845 discretized volumes throughout the core). This discretization is different from that is used for the material composition tracking (presented in Figure 7(b) and Figure 8(b) and identifined as zones), and is used only for power and fission density tracking. It is important to note that all MCNP calculations completed as part of this work have an inherent statistical uncertainty due to the Monte Carlo solution approach. Power distribution statistical uncertainties reported by MCNP have been performed to be less than 2 % (1-sigma) in power regions.

Assembly-wise normalized power distributions are presented in Figure 16 for SU, BOC, MOC, and EOC states. The power distribution calculations are performed for the BOC state to observe the effect of the Xe-135 build-up in the core. The assembly-wise maximum and the minimum power peaking values throughout the cycle are calculated as 1.12 and 0.90, respectively, both are found at the EOC state. More power is produced in the second cycle FAs, namely C'11, B'23 and A'31 (refer to Figure 9 for locations), due to the fact that the fresh Cd burnable absorbers placed in the side plates of the FAs suppress the neutron flux in the reactor center. It can be observed and the effect of the Cd burnable absorber on the flux suppression decreases up to the MOC state and after. As a result of depleted Cd burnable absorber, the inside-to-outside core loading pattern, and the withdrawal of the control blades during the operating cycle, more power is produced in the freshly loaded FAs (A12, B22, C32) in MOC and after. For a possible limiting condition, the maximum generated assembly power is calculated as 2.49 MW with corresponding local assembly-wise power peaking factor of 1.12 in the B22 fuel assembly at the EOC state.

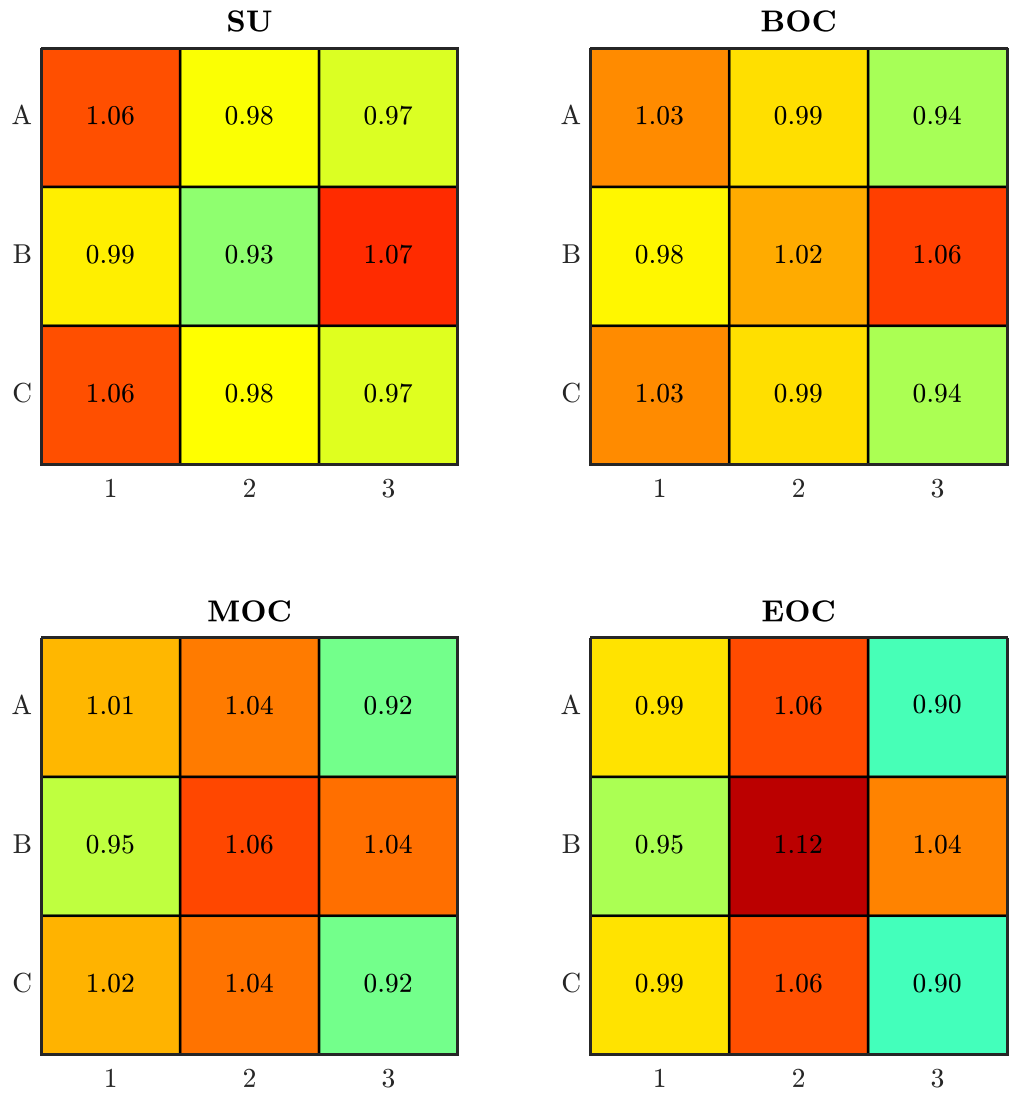

Figure 16. Normalized power heatmap of the assemblies in the cycle states.

Figure 17 shows axially-averaged transverse power distribution of all fuel stripes inside the FPs along axial fuel length. As seen in Figure 17, higher local stripe power peakings occur at the outer region of the 2nd cycle FAs for SU and BOC states. At SU and BOC, these higher power peaking values are due to the two FAs placed in the two western corners of the reactor (C'11 and A'31), which contain more U^{235} than the FA located in the east-central part (B'23). But the reentrance window orientation of the CNSs affects the formation of higher peak locations to a lesser extent. The hottest axially-averaged stripe power peaking value is observed in the 1st plate's 1st stripe, which is shown in the corner-most region of the C'11 FA in Figure 17; this exhibits a power peaking value of 1.75 at the SU state.

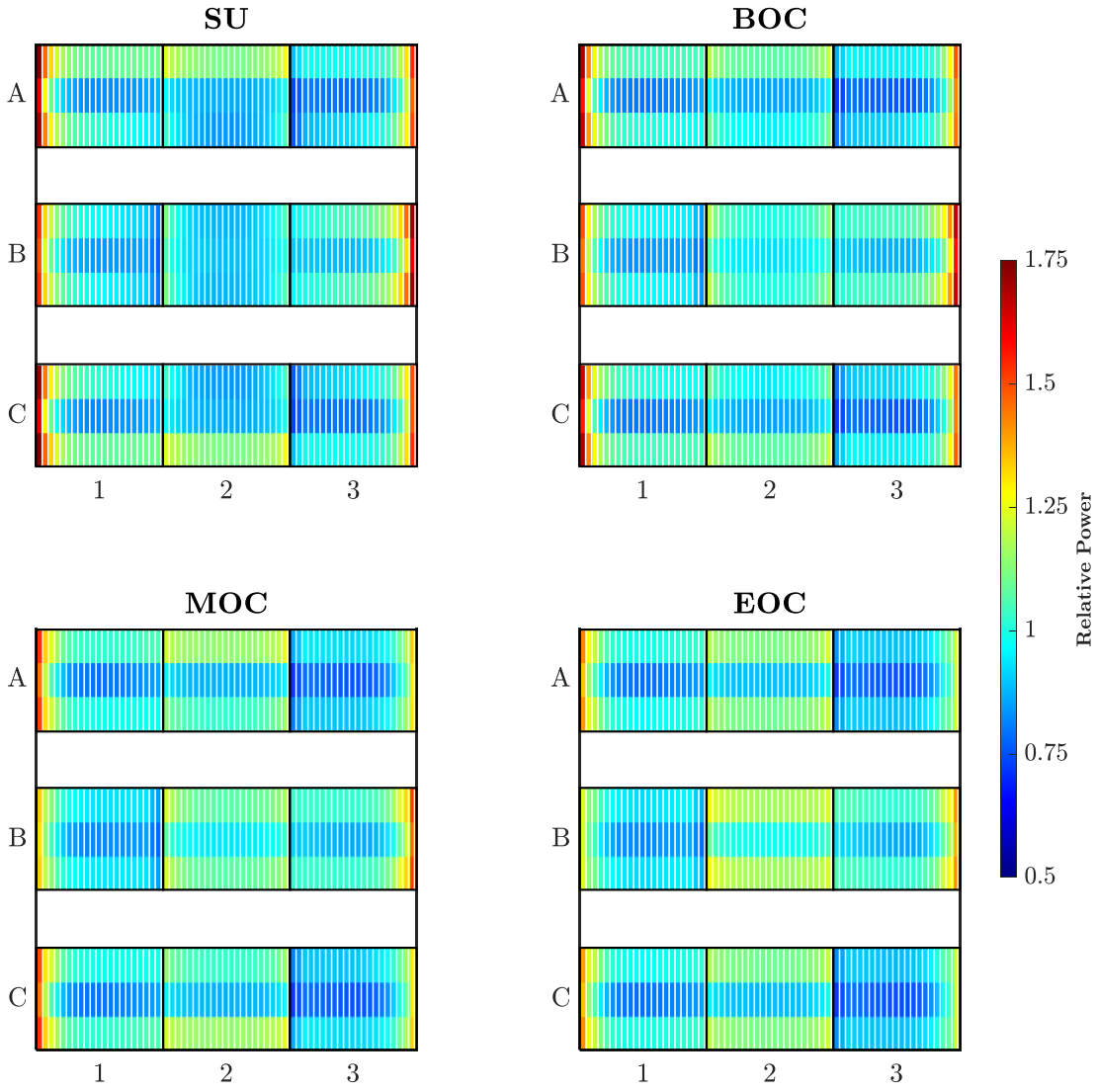

Figure 17. Normalized power heatmap of the stripes in the cycle states.

In the normalized power heat map shown in Figure 17, the greatest axially-averaged transverse power peakings is observed in either the 1st plate or 21st plate. The normalized power distribution of the 1st and 21st plates are shown in Figure 18 for all cycle states. Unlike Figure 17, the highest local power generation occurs at the outer region of the 2nd cycle FAs for the BOC state (the 1st plate). The maximum local peaking value is calculated 1.98 at the assembly C'11.

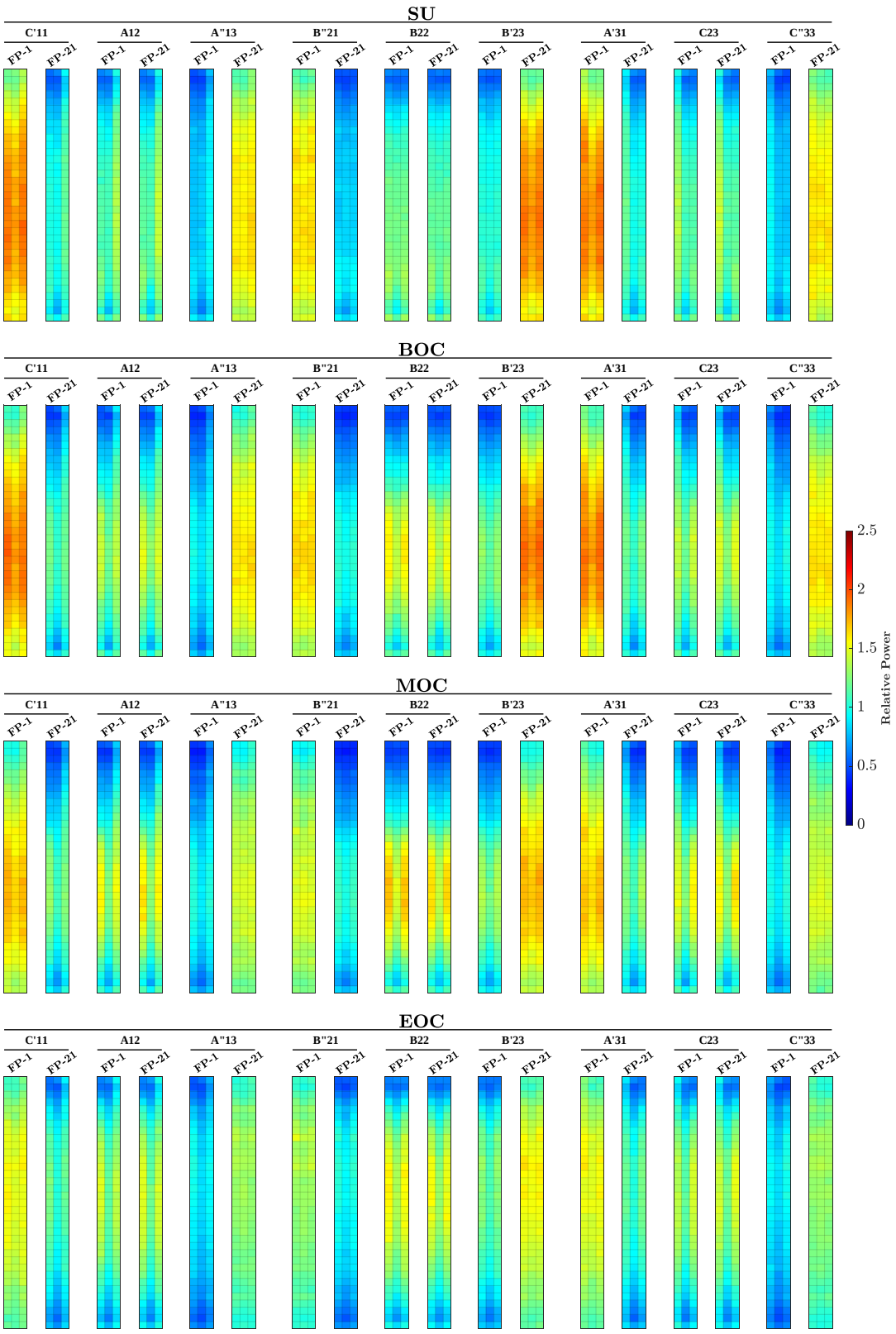

Figure 18. Normalized power heat map distribution of the 1st and 21st plates' stripes in the cycle states.

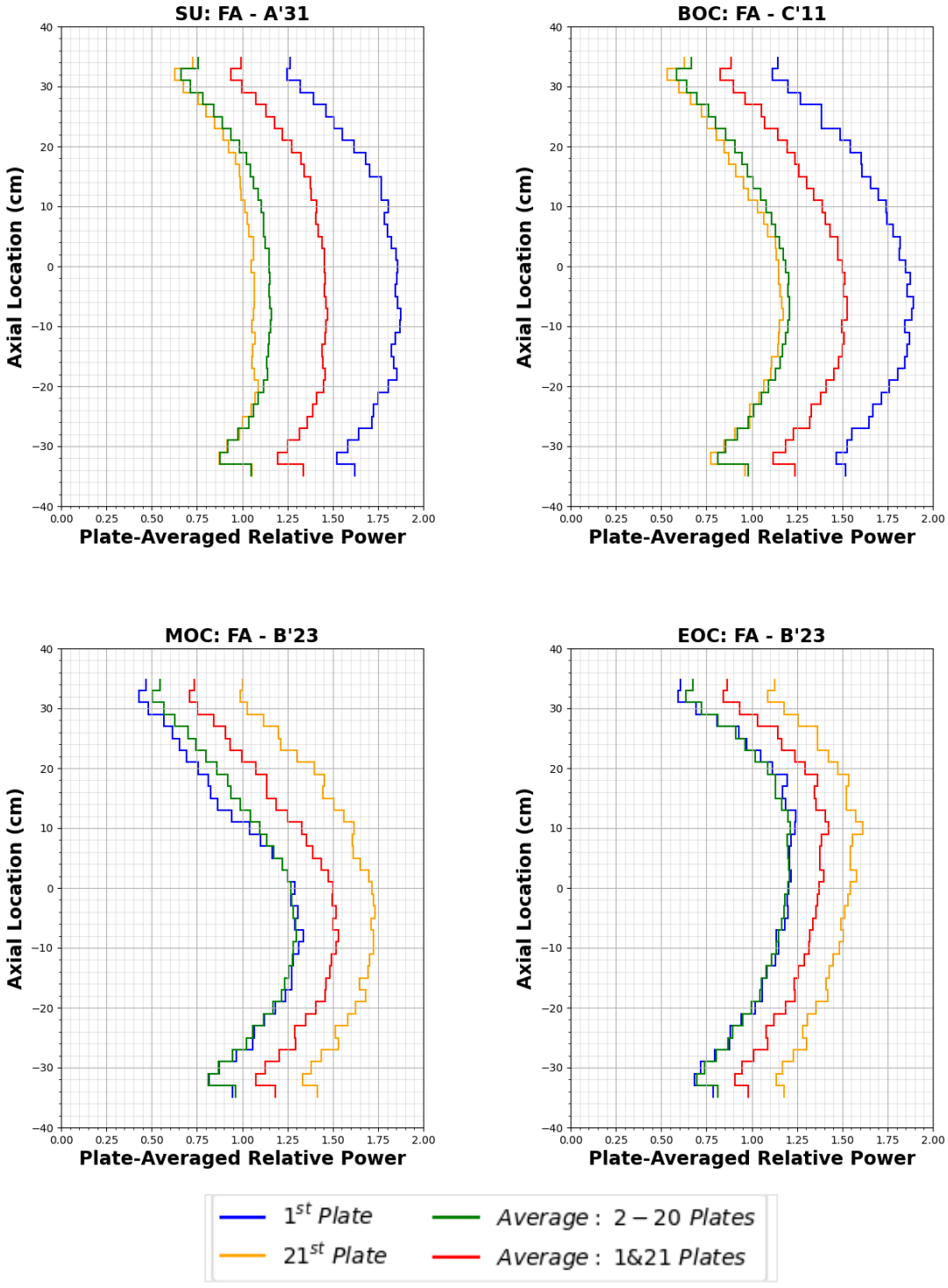

Figure 19. The axial power distribution of 1st plate, 21st plate, inner 19 plates' average, and all plates average at cycle states.

All calculations show that the outer plates yield more heat generation than the inner plates in the assemblies. Hence, the outer plates encounter additional thermal neutron flux due to moderation from the coolant around the peripheral clearance of the core. This phenomenon is exaggerated by the presence of the heavy water reflector around the core. Heavy water tank reflects thermal neutrons and results in an increase of the fission density of the outer plates. While it is valuable to observe the axial power distribution of the outer plates in Figure 18, the axial power distribution of the other plates in the assemblies can also be reviewed. Figure 19 shows for all cycle states: the axial power distributions for the 1st plate, 21st plate, averaged inner plates (2 to 20), and average power over all plates. The highest average peak value of the axial power is determined to be 1.89 in the 1st plate of the C'11 assembly at the BOC state.

Another limiting condition of a research reactor design is the local power and fission densities in the FPs. Power densities are calculated as the power of the fuel divided by its volume for any given cycle state (SU, MOC, etc.). Local fission densities are calculated by assuming that the cycle state's power is changing linearly in the period between subsequent cycle states, where the number of fissions is assumed to vary linearly with power. So, the fission densities correspond to the total number of fission events that occur between two subsequent cycle states, or in any given period. The power and fission densities of all fuel nodes in the model are plotted in Figure 20 with coloring based on the cycle number, and in Figure 21 with coloring based on the cycle state. In Figure 20, the cycle numbers represent an assembly's residence time inside the core (fresh fuels are 1st cycle FAs; twice-burned fuels are 3rd cycle FAs). Per the green (1st cycle) dots in Figure 20, the freshly loaded Cd absorber wires cause flux suppression in the 1st cycle FAs. For these FAs, lower peak-power densities of ~16 kW/cm^3 are observed compared to the absolute peak-power densities of ~18 kW/cm^3 in the 2nd cycle FAs. Due to having depleted Cd wires, elevated peak-power densities for 2nd cycle FAs are observed with values of ~18 kW/cm^3; and they are accompanied with local fission densities in the range of 1.5×10^{21} fission-cm^{-3} to 2×10^{21} fission-cm^{-3}. The 3rd cycle FAs have the highest fission densities at 3×10^{21} fission-cm^{-3} with lower peak-power densities due to decreasing amounts of uranium and increasing fission-yielded parasitic isotopes throughout the cycle length. The absolute maximum fission density computed is 4.5×10^{21} fission-cm^{-3} in the 3rd cycle FAs.

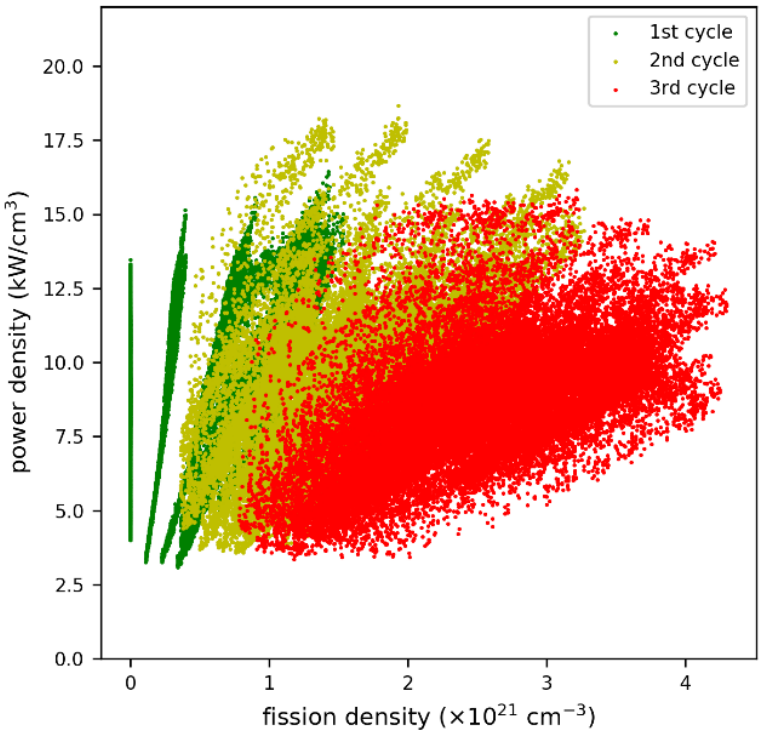

Figure 20. Power density as a function of fission density for the whole core at equilibrium.

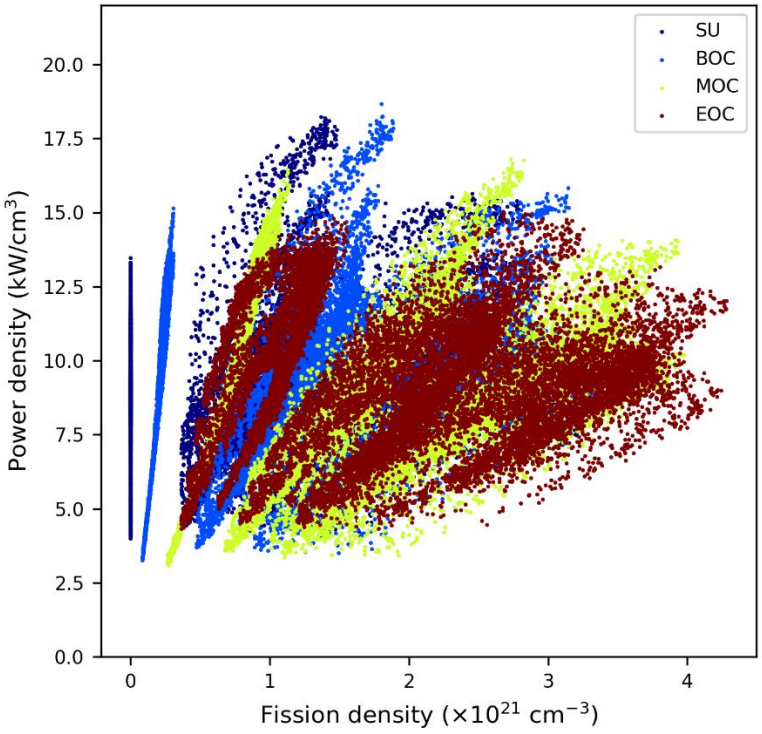

Figure 21. Power density as a function of fission density for each node by cycle state with an equilibrium core.

Figure 20 and Figure 21 provide an understanding of the relationship between the peak power and fission densities, which is useful for comparisons with other US High-Performance Research Reactors (USHPRRs) that are considering the use of U-10Mo LEU fuel (shown in Figure 22) [11, 12]. Figure 22 shows preliminary design calculations for the USHPRRs that are considering a conversion from their existing HEU fuels to U-10Mo LEU monolithic fuel. , The inside of the dashed yellow lines in Figure 22, represents the projection of the values of Figure 20, which can be referred to as the performance envelope of the NNS. The NNS envelope reaches a power density that is near double that of the NBSR's maximum power density, but it still operates at lower power densities than the Advanced Test Reactor (ATR) when considering similar fuel, other than a somewhat thinner NNS fuel plate. As in Figure 22, the ATR, with three pump operation (ATR-3 Pump), and the NBSR determine the bounds of power density and fission density limits for USHPRRs for U-10Mo LEU fuel [13].

It is important to note that the power density and fission density values for the reactors represented in Figure 22, along with the geometry of the fuel core thicknesses for these reactor designs, are being used as the bases of target test values for planned plate- and element-level irradiation testing for qualification and demonstration of the U-10Mo fuel that is being completed under the scope of the USHPRR Conversion Project. This testing of the U-10Mo power density and fission density bounds the NNS design, although, as stated above, the NNS fuel plate geometry is somewhat thinner than that of the NBSR LEU fuel plates which are irradiated to the greatest power and fission density values.

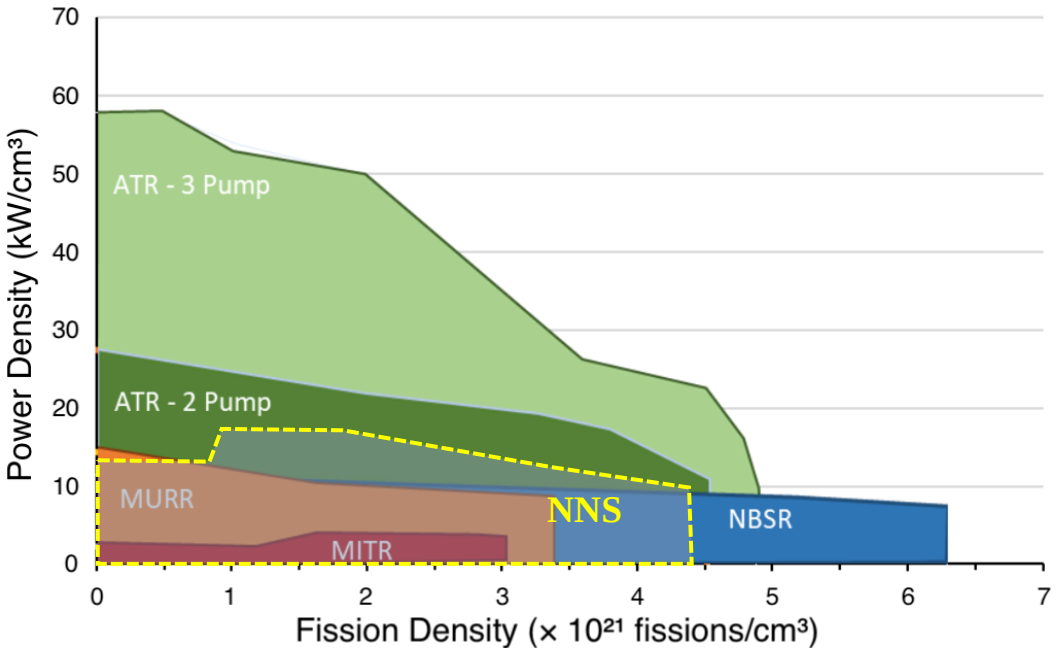

Figure 22. Power and Fission Density Profiles in other USHPRRs considering U10-Mo LEU conversion (modified and reproduced from [11, 12]).

3.3. Reactivity of Control and Safety Blades, and Shutdown Margin

The primary neutron poison to control and shutdown the reactor is hafnium in all control and safety blades. The orientation and locations of the control and safety blades are shown in Figure 23. The safety blades are labeled from 1 to 4, while the control blades are labeled A and B (A marks the blade between FA rows A and B; and B marks the blade between FA rows B and C). In normal operation, all safety blades are withdrawn from the core, and the reactor is controlled by adjusting the A and B control blades.

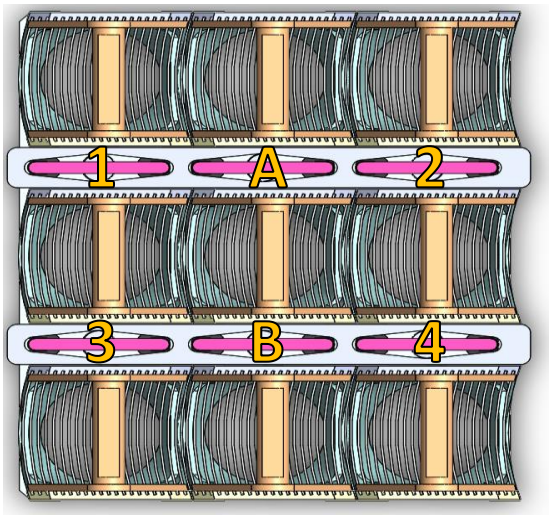

Figure 23. Control and Safety Blades Orientation (Top view).

To safely shut down the reactor and maintain a safe shutdown state, it is important to determine the reactor shutdown margins for the equilibrium core conditions. To determine those margins, various predetermined control and safety blade configurations (listed in Table 4 and Table 5) are arranged for investigation. The k_{eff} are obtained for the configurations to determine their reactivities relative to the critical core's configuration (when $k_{eff} = 1$). Table 4 and Table 5 show the k_{eff} and core reactivity behavior for all configurations of control and safety blades at the SU and EOC states, respectively. Cases #1 and #9 are when all control and safety blades are at withdrawn and at fully inserted, respectively. Cases #2 and #3 correspond to configurations where all safety blades and one of the control blades is fully withdrawn and only one of the control blades is fully inserted. Case #4 corresponds all safety blades withdrawn and both control blades being fully inserted. The remaining Cases #5 through #8 simulate the stuck-blade criterion, where both control blades are fully withdrawn with any one of the safety blades, while the other three safety blades are completely inserted in the core. All calculations are performed at the most reactive state in the cycle (i.e., SU with three freshly loaded FAs and no ^{135}Xe poison) and the least reactive state point in the cycle (i.e., EOC by eliminating the ^{135}Xe poison concentration from the nuclear fuel composition).

Any individual safety blade creates similar reactivity feedback when fully withdrawn with the control blades. Although all k_{eff} results stay within the uncertainty of k_{eff} values (all uncertainty values are less than 20 pcm) for stuck-blade analysis, the most severe stuck-blade condition is

observed when the #2 safety blade is fully withdrawn (i.e., stuck out)at SU in Case #6. For Cases #5 through #8, the reactor has sufficient margin to safely shut down the core. Therefore, the shutdown margins of the safety blades are satisfying the design target established in section 1.1 and demonstrate that any three of the four safety blades are sufficient to induce subcriticality at any cycle state. Even if the most effective safety blade (which is expected to be safety blade #2 at the most reactive state SU) is fully withdrawn, the remaining safety blades yield sufficient negative reactivity to shut down the reactor. All calculations show that the reactor has sufficient shutdown margin to meet the criteria in section 1.1 and the "stuck blade" criterion from NUREG-1537 [5] and ANSI/ANS-15.1 [14].

Table 4. Core reactivity values for various blade configurations at the SU state†.

Blade Configuration			$k_{\mathbf{eff}}$	$\Delta\rho$ (%)	$\Delta\rho$ (pcm)
Case #	**Withdrawn**	**Inserted**			
1	1, 2, 3, 4, A, B	--	1.06001	5.66	5661
2	1, 2, 3, 4, B	A	1.02445	2.39	2387
3	1, 2, 3, 4, A	B	1.02364	2.31	2309
4	1, 2, 3, 4	A, B	0.98602	-1.42	-1418
5	A, B, 1	2, 3, 4	0.95892	-4.28	-4284
6	A, B, 2	1, 3, 4	0.95949	-4.22	-4222
7	A, B, 3	1, 2, 4	0.95938	-4.23	-4234
8	A, B, 4	1, 2, 3	0.95879	-4.30	-4298
9	--	1, 2, 3, 4, A, B	0.86729	-15.30	-15302

†The $\Delta\rho$ values are calculated as deviation from unity.

Table 5. Core reactivity values for various blade configurations at the EOC state†.

Blade Configuration			$k_{\mathbf{eff}}$	$\Delta\rho$ (%)	$\Delta\rho$ (pcm)
Case #	**Withdrawn**	**Inserted**			
1	1, 2, 3, 4, A, B	--	1.04402	4.22	4216.39
2	1, 2, 3, 4, B	A	1.00010	0.01	10.00
3	1, 2, 3, 4, A	B	1.00042	0.04	41.98
4	1, 2, 3, 4	A, B	0.95323	-4.91	-4906.48
5	A, B, 1	2, 3, 4	0.92607	-7.98	-7983.20
6	A, B, 2	1, 3, 4	0.92505	-8.10	-8102.26
7	A, B, 3	1, 2, 4	0.92521	-8.08	-8083.57
8	A, B, 4	1, 2, 3	0.92613	-7.98	-7976.20
9	--	1, 2, 3, 4, A, B	0.83416	-19.88	-19881.08

†The $\Delta\rho$ values are calculated as the deviation from the unity

Figure 24 shows the integral reactivity worth as a function of the banked control blade position inside the core for each cycle state. As in the figure, the total integral worth of the control blades increases as the cycle progresses because these blades are next to the burnable poison wires that

burn out during the cycle. The depletion of burnable poisons in the FAs is expected to result in an increase in the thermal flux in assemblies A12, B22, and C32 during the operating cycle, and that phenomenon will create an increment of the effectiveness of the control blades. The situation with the safety blades is different and their worth does not change much during the cycle. The total integral worth of the control blades is ~7.1 % $\Delta\rho$ at the fully withdrawn position in the SU state and ~9.3 % $\Delta\rho$ at the EOC state.

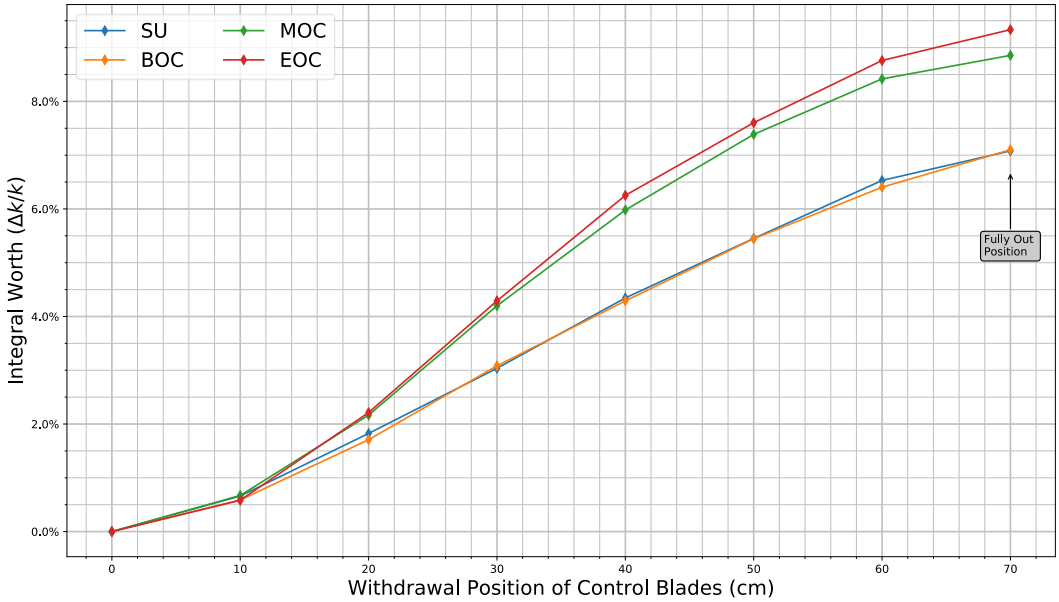

Figure 24. Integral reactivity of the control blades in the cycle states.

The integral worth of the banked safety blades as a function of the withdrawal position is shown in Figure 25. While calculating the safety blades' integral worth, it is assumed that the control blades are fully inserted into the core and the results are obtained by changing the position of the safety blades in the core. Similar to the control blades' behaviors, the safety blades' worth increases as the EOC is approached. The total integral worth of the safety blades is calculated 13.89 % $\Delta\rho$ and 15.28 % $\Delta\rho$ for SU and EOC, respectively.

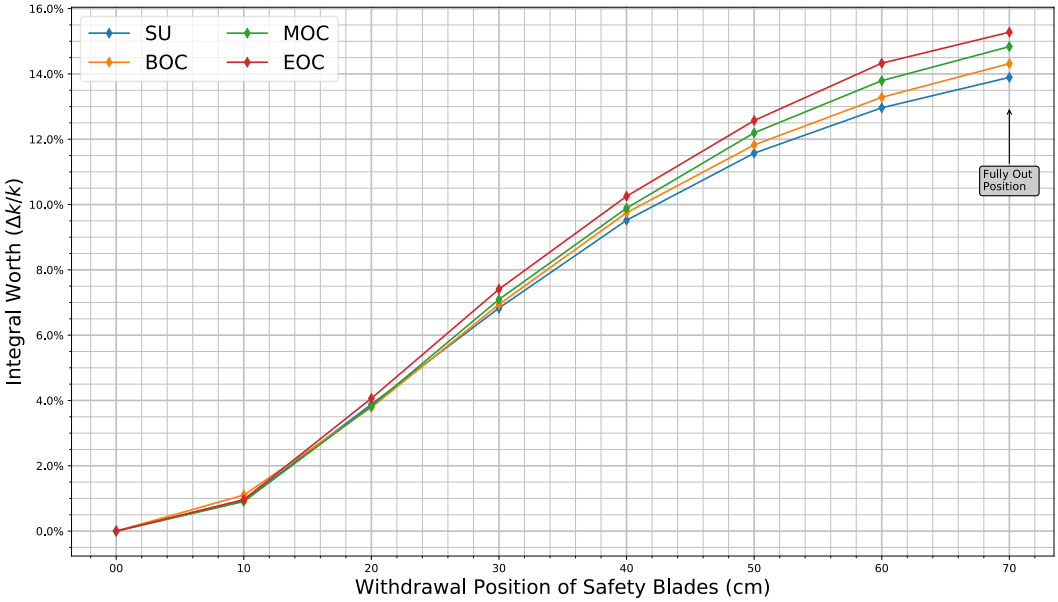

Figure 25. Integral reactivity of the safety blades in the cycle states.

3.4. Reactivity Coefficients (Fuel Temperature, Coolant/Moderator Temperature, Void, Mixing)

This section focuses on the inherent safety characteristics of the NNS, where the fuel temperature coefficient, coolant/moderator temperature coefficient, void coefficient, and mixing coefficient are demonstrated to be negative for the SU and EOC at ECS.

Unless stated, all calculations assumed banked control blades (both moving together) where both control blades are maintained at the estimated critical positions (ECP). The ECP is the position of control blades where the core becomes critical (at $k_{\text{eff}} = 1$). The determined ECPs are tabulated in Table 6 for each cycle state.

Table 6. The estimated critical positions of control blades at each cycle state while safety blades are fully withdrawn (at 70 cm).

	Cycle State			
	SU	BOC	MOC	EOC
Control Blade Estimated Critical Position (cm)	16.76	45.46	44.84	64.74

3.4.1. Fuel Temperature Coefficient

Although the Doppler reactivity effect of the NNS is not expected to be as large as power reactors due to a small temperature gradient across the very thin fuel thickness and the calculated average fuel temperature inside the fuel is ~75 ºC, the Doppler reactivity coefficient of the NNS has been calculated the using On-The-Fly (OTF) Doppler Broadening (OTFDB) option included in MCNP6. The 485 OTF data files were created by using the ENDF/B-VIII.0 cross-section data libraries for use in MCNP. Meanwhile, it should be noted that the runs performed by using OTF has calculated approximately 150 pcm higher in k_{eff} at 20ºC than what was calculated with the original 20ºC cross-sections which are directly generated by LANL. The difference may arise from either propagated fit errors of the OTF files or broadening of the absorption cross-sections of moderator, reflector and cryogenics that are used in the CNSs. Further investigation will be performed by generating the cross-sections at the operating conditions in the future.
The calculations show that average reactivity of the reactor decreases 7 pcm with the increasing per Celsius degree temperature. The calculated total Doppler reactivity change from cold state to the hot full power state due to temperature increase in the fuel core is 385 pcm (0.39 $\%\Delta\rho$).

3.4.2. Moderator/Coolant Temperature Coefficient

In safety assessments of thermal reactors, the moderator temperature coefficient of reactivity (MTC) is an important factor to consider. The NNS core uses light water as both moderator and coolant between the FPs. It is also surrounded by a heavy water reflector tank. The light water moderator temperature is important to maintain effective thermalization of the fission neutrons. An increase in the moderator temperature reduces its density and its effectiveness in thermalizing the fission neutrons, which decreases the total amount of fission events in the system. The MTC quantifies the change in reactivity due to changes in the light water temperature. A negative coefficient (i.e., negative reactivity feedback) is desirable to ensure reactor stability such that an increase in moderator temperature causes a reduction in the criticality of the system if an unanticipated water temperature increase occurs. At the initial state of the neutronics design, the NNS core design be in an under-moderated condition while doing initial cell calculations. A negative MTC is one of the evidence of an under-moderated core design.

Figure 26 illustrates the core's $\%\Delta\rho$ as a function of the moderator temperature at SU and EOC. As the moderator is heated from 20°C to 90°C, the average MTC is -0.017 $\%\Delta\rho$/°C and -0.015 $\%\Delta\rho$/°C at SU and EOC states, respectively. The average MTC behavior is almost linear with a negative slope as a function of increasing moderator temperature.

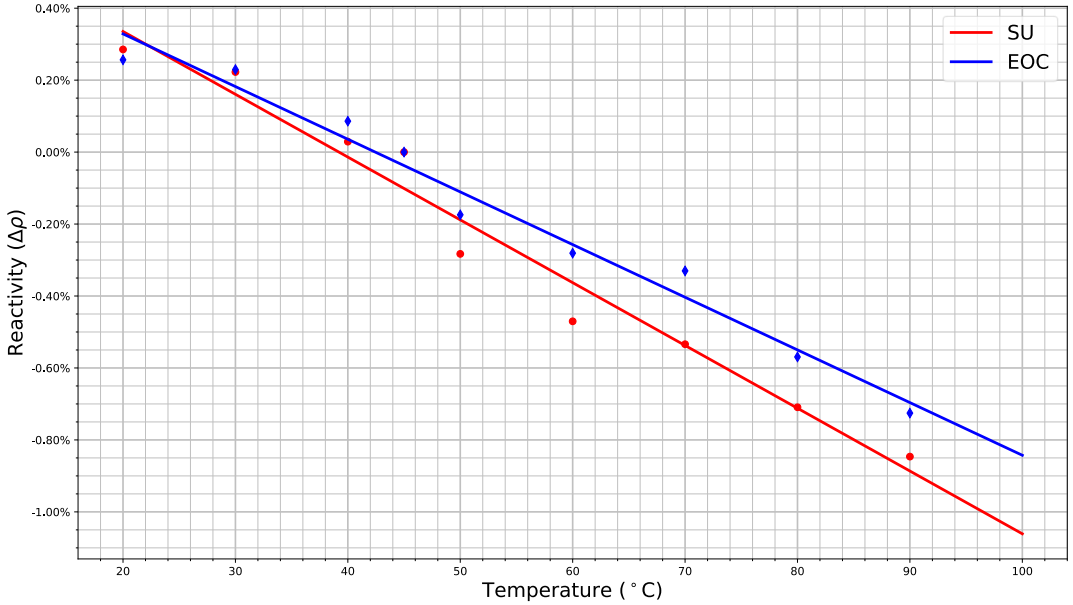

Figure 26. The core's %$\Delta\rho$ as functions of moderator temperature at SU and EOC.

3.4.3. Void Coefficient

If the water heats enough to cause voids in the system through boiling, or if other gases in the system build enough to cause similar voids, such void formation will cause reactivity feedback in the core. The void coefficient is the reactivity feedback due to a change in the atom density caused by void formation. Similar to the MTC, multiple simulations are run to investigate the effects of voids in the system, which can be emulated by varying the density change that contains partial void of the moderator independent from moderator temperature. The results show a negative reactivity for any void formation, where the average void coefficient during the SU state is -0.253 %$\Delta\rho$/%-void and -0.234 %$\Delta\rho$/%-void at the EOC state as seen in Figure 27.

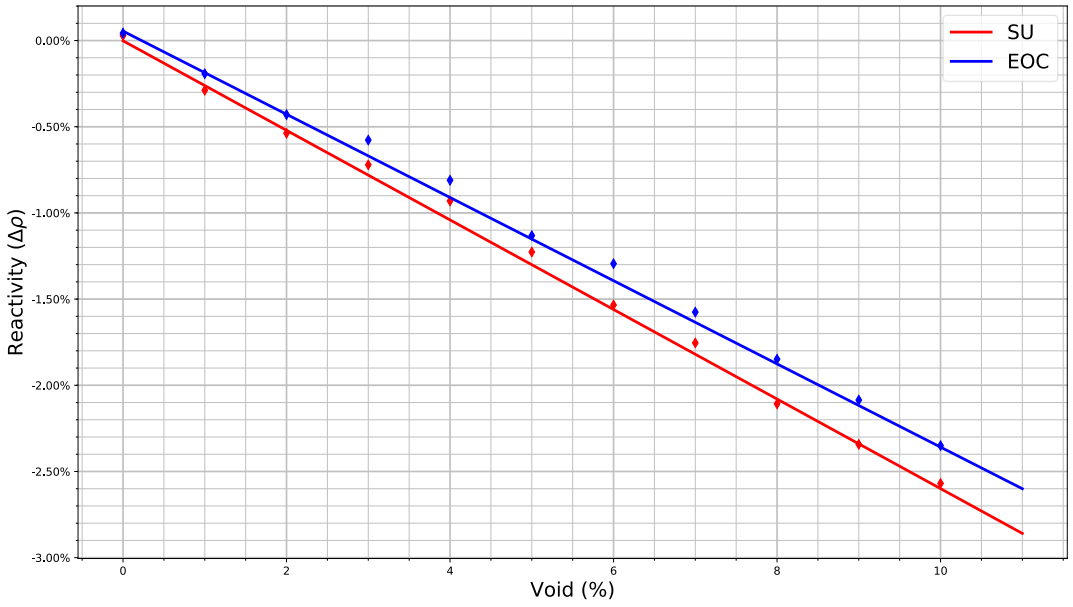

Figure 27. Core %$\Delta\rho$ as functions of moderator void at SU and EOC.

3.4.4. D_2O and H_2O Water Mixing Coefficients

There are two mixing mechanisms inside the NNS. One is heavy water (D_2O) ingress into the reactor pool and the other is light water (H_2O) ingress into the reflector tank. Both cases are investigated in terms of their reactivity effects on the reactor. The analyses are performed in the most and least reactive states of the cycle, at SU and EOC. Theoretically, the complete replacement of both H_2O and D_2O is not possible; however, the analyses consider D_2O or H_2O ingress (to the other system) from 0 % to 99 % with increments of 10 %. The density change of the mixture was computed by considering the atomic percentage change of the H_2O and D_2O mixture. Mixture density and material composition are defined in the MCNP model as a function of the mixture's atomic ratio, where homogeneity of the mixture is assumed in all cases. The temperature of both D_2O and H_2O in these analyses is the average operating temperature of 46 ºC. Thermal scattering libraries at the nearest temperature of the heavy and light water are also used in the model.

3.4.4.1. Heavy Water Ingress into Reactor Primary System

The first part of the mixing coefficient analysis is the D_2O ingression into the reactor primary cooling system, which only contains H_2O. Notice in Figure 28 that as the D_2O content increases in the reactor primary cooling system, the reactivity decreases and yields a negative mixing reactivity coefficient. Even if the entire H_2O primary system is replaced with D_2O (which is unlikley in the NNS design), the system's reactivity continues to decrease, and the reactor would inherently shut down due to the overwhelming negative mixing reactivity coefficient. The average reactivity changes in the system per atomic percentage change in heavy water in the primary are calculated -0.225 %$\Delta\rho$/atom% and -0.201 %$\Delta\rho$/atom% at SU and EOC, respectively.

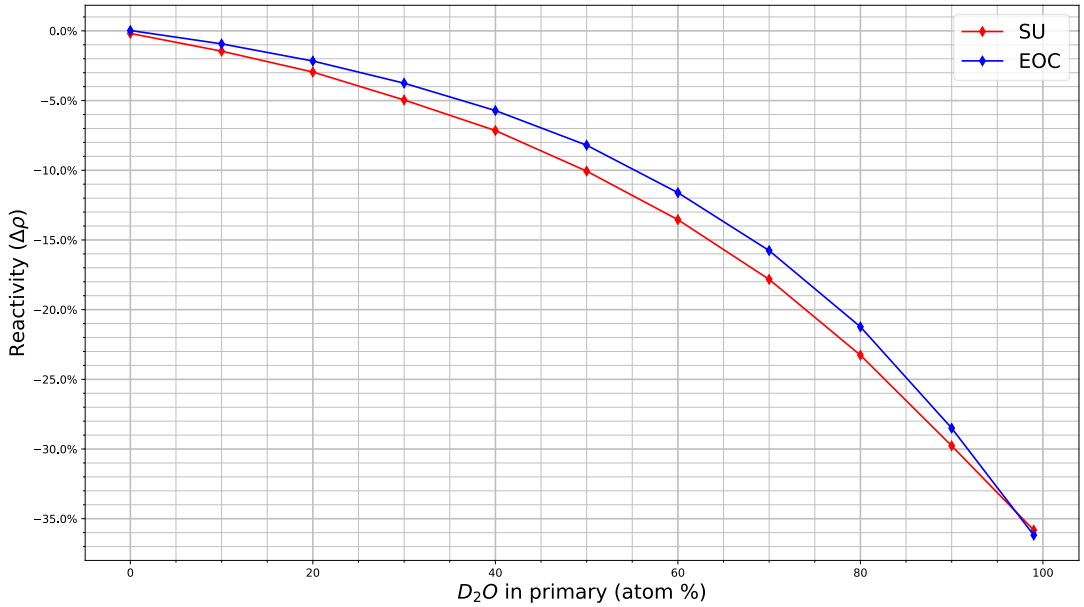

Figure 28. Core $\%\Delta\rho$ as a function of D_2O percentage in the primary system at SU and EOC.

3.4.4.2. Light Water Ingress into the Reflector

The effects of H_2O ingression into the reflector tank are investigated in this section. As H_2O begins ingress into the reflector tank, the high absorption cross-section of hydrogen will reduce the effectiveness of the reflector tank and cause a drop in reactivity. This is reflected in Figure 29, where increasing H_2O content in the reflector tank causes a considerable drop in reactivity. Continuous H_2O ingression into the reflector tank inherently shuts down the reactor due to the significant negative reactivity feedback. The average reactivity change in the system per atomic percentage change in light water in the reflector tank is -0.245 $\%\Delta\rho$/atom% at SU and -0.214 $\%\Delta\rho$/atom% at EOC.

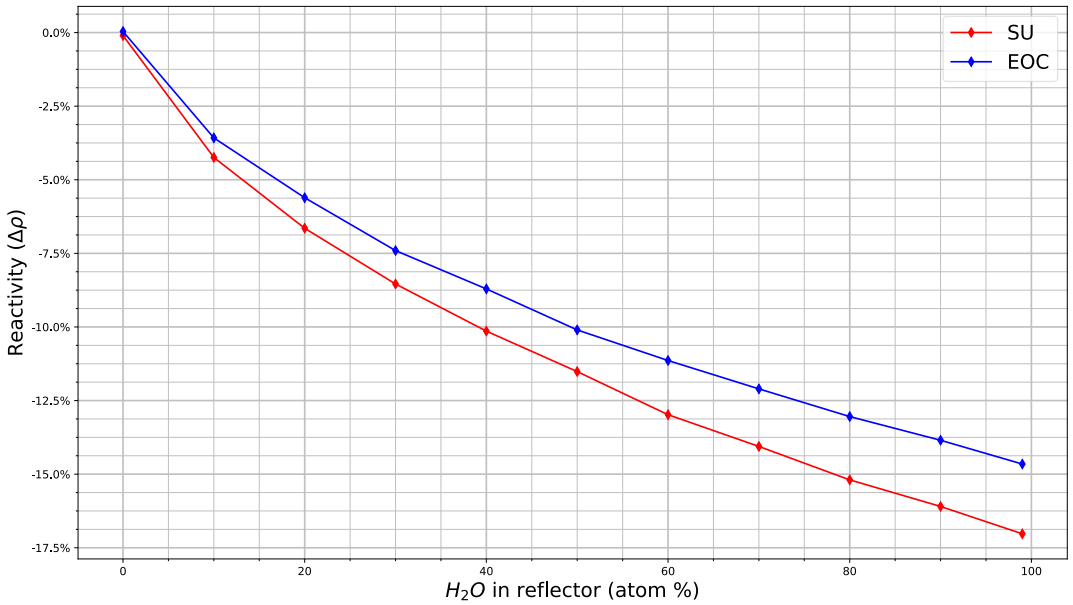

Figure 29. Core %$\Delta\rho$ as a function of H_2O percentage in the reflector at SU and EOC.

3.4.5. Reflector Dump

The reflector tank is a D_2O-filled cylindrical tank that is 130 cm in height. In emergency situations applying the secondary shutdown system, the half of the D_2O in the reflector tank would be dumped and replaced with He in ~10 seconds to induce a subcritical core. Figure 30 shows the effects of variations in the reflector tank's dump level on reactor reactivity. The first ~30 cm of the dumped level does little to affect the system's reactivity. However, after dumping ~50 cm of reflector content, the negative reactivity insertion of the dumped D_2O would be capable of compensating the total excess reactivity of the core at the SU state. As in Figure 30, when the total reflector content is dumped from the system, -47.6 %$\Delta\rho$ and -41.3 %$\Delta\rho$ reactivity feedbacks are evaluated at SU and EOC, respectively. This demonstrates that the reflector dump can induce subcriticality in the reactor at any cycle state.

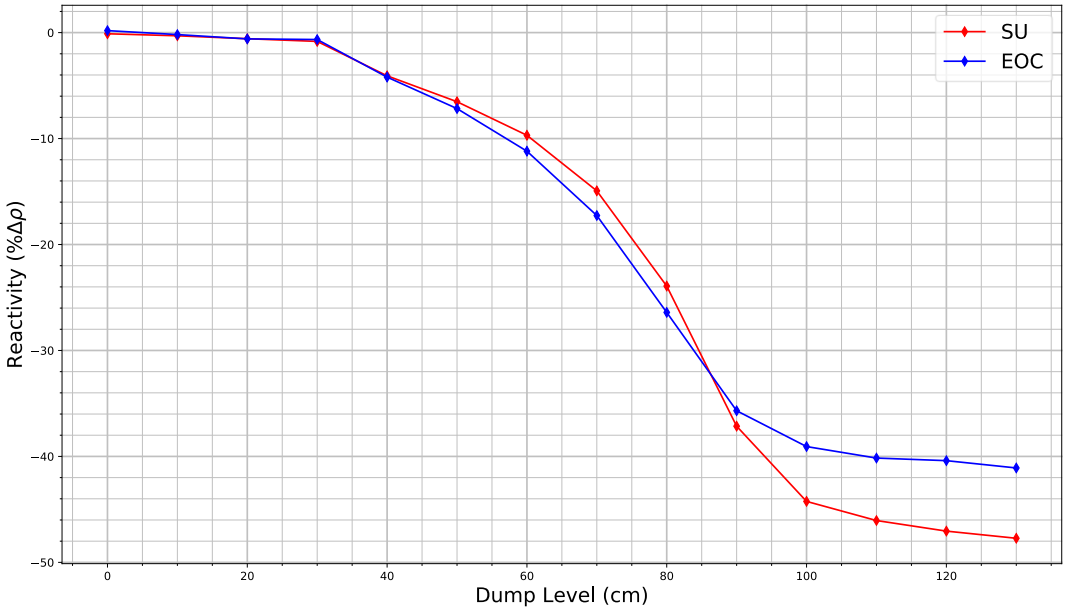

Figure 30. Reflector Dump Level vs. Reactivity Change.

3.5. Reactor Kinetics Parameters

In a nuclear reactor, when neutrons are absorbed by fissile (U-235 in this case) nuclides, energy, and two to three neutrons are released. The U-235 breaks into two smaller atoms called fission products. The majority of the emitted neutrons are prompt neutrons, which release instantly as opposed to delayed neutrons, which release during some time interval (milliseconds to minutes) after fission occurs.

The analysis of a reactor transient depends on: the delayed neutron fraction of each delayed neutron group (β_i); the prompt neutron lifetime (l_p); and the decay constants of each delayed neutron group (λ_i). Those delayed neutron kinetics parameters and the control/safety blades' worth (calculated in the previous sections) are used in the safety analyses of research reactors. To obtain the kinetic parameters, the KOPT card is activated in the MCNP model, which enables the code to generate the required kinetic parameters of the system, such as prompt neutron generation time (Λ), β_i, and λ_i. It should be emphasized that Λ and l_p used interchanged if and only if the system is critical; otherwise, the relation $\Lambda = l_p/k_{eff}$ should be used to convert from neutron generation time to prompt neutron lifetime. Considering a critical system at each cycle state, Table 7 shows the resulting Λ in μs alongside its uncertainty.

Table 7. The prompt neutron generation time and its uncertainty for each cycle state for a critical system.

Cycle state	Generation Time, Λ (μs)	Generation Time Uncertainty, σ_Λ (μs)
SU	260.22	8.60
MOC	234.38	7.40
EOC	236.71	8.16

The remaining kinetics parameters are shown for SU and EOC for ECS in Table 8 and Table 9, respectively. The β_{eff} is calcualted higher than the pure U-235 value and it seems to decrease from the SU to the EOC state. It is an expected value of change in a HALEU loaded reactor because the delayed neutron fraction of Pu-239 is 0.002, and it tends to decrease the fraction of delayed neutrons. Although there is a difference in β_{eff}between SU and EOC, it is small enough to consider an average of the two as an appropriate estimate, where β_{eff} of the reactor is approximately 0.00644±0.00044.

Table 8. The decay constants and effective delayed neutron fractions during the SU state.

SU			
Group	$\boldsymbol{\lambda_i(1/s)}$	$\boldsymbol{\beta_i}$	**Relative Uncertainty σ_β**
1	0.01334	0.00035	0.00015
2	0.03269	0.00136	0.00034
3	0.12073	0.00088	0.00025
4	0.30318	0.00289	0.00041
5	0.85177	0.00059	0.00014
6	2.86021	0.00048	0.00016
$\beta_{eff} = \sum \beta_i$		0.00655	0.00064

Table 9. The decay constants and effective delayed neutron fractions during the EOC state.

EOC			
Group	$\boldsymbol{\lambda_i(1/s)}$	$\boldsymbol{\beta_i}$	**Relative Uncertainty σ_β**
1	0.01334	0.00022	0.00010
2	0.03268	0.00089	0.00021
3	0.12073	0.00076	0.00019
4	0.30318	0.00279	0.00042
5	0.85194	0.00130	0.00027
6	2.85903	0.00036	0.00012
$\beta_{eff} = \sum \beta_i$		0.00632	0.00059

4. Summary & Conclusions

In this report, we investigated the nuclear criticality safety and reactor operation characteristics (from a neutronics and fuel management perspective) of the NNS core with its reflector, including beam tubes and cold neutron sources. The equilibrium core neutronics characteristics were calculated throughout a typical cycle with the MCNP 6.2 code package using the ENDF/B-VII.1 and ENDF/B-VIII.0 cross-section data libraries. The reactor shall be designed to operate with a safety-first principle allowing reliable operation and ease of maintenance where possible.

The power peaking distributions were computed throughout various locations in the core at different states to provide an understanding of the fuel heating. The maximum generated assembly power is 2.49 MW with a relative power peaking at 1.12 in the central (B22) assembly at the EOC state. This is an expected result because of the depletion of the Cd wires in the fresh fuel element, and the fuel loading configuration designed as an in-out core loading pattern, which results in the maximum power peaking occurring at the EOC state.

The hottest stripes are found at the periphery of the FAs. This is attributed to the improved neutron moderation offered by the water gap between the chimney and the plate. This gap is larger than the other coolant channels and offers improved moderation of neutrons. This power peaking can be attributed to the reflected thermal neutrons coming from the reflector tank. The maximum local peaking value calculated is 1.98 and the highest peak value of the axial power is 1.89 at the assembly C'11 for the BOC state. Further, the hottest stripe power peaking value is in the 1st plate's upper region of the same assembly with a power peaking value of 1.75 at the SU state.

To understand the operational envelope of the NNS and how it fits within the existing USHPRRs, the power and fission densities of the fuel in the NNS were obtained for each cycle and each discretized fuel geometry. The highest power density observed is ~18 kW/cm^3 in the 2nd cycle FAs. The local fission densities for the 2nd cycle FAs are found within the range of 1.5×10^{21} cm^{-3} to 2×10^{21} cm^{-3}. The 3rd cycle FAs have the maximum fission densities in the core as expected, and the highest value calculated is 4.5×10^{21} cm $^{-3}$. Therefore, the operational envelope of the NNS is covered by power density and fission density limits for the USHPRRs LEU conversion study [11, 12]. Fuel qualification and demonstration testing of the U-10Mo fuel being completed under the scope of the USHPRR Conversion Project bounds the power density and fission density of the NNS design, although the NNS fuel plate geometry is somewhat thinner than that of the U-10Mo fuel plates which are planned to be irradiated to the greatest power and fission density values.

To understand the NNS core's reactivity safety margins and ensure compliance with the stuck-blade criterion from NUREG-1537 [5] and ANSI/ANS-15.1 [14], various control and safety blade withdrawal combinations were analyzed. Calculations showed that the NNS has sufficient margin to safely shut down the reactor during a stuck-blade event at any cycle state.

To assess the criticality safety of the NNS, the coolant/moderator temperature, void, mixing of reflector water, and pool water reactivity coefficients are calculated. The computed moderator temperature coefficient of reactivity is -0.017 %$\Delta\rho$/ºC and -0.015 %$\Delta\rho$/ºC at SU and EOC, respectively. When a void is formed in the NNS primary, it creates a negative reactivity in the system, where the average void coefficient of reactivity is -0.253 %$\Delta\rho$/%-void and -0.234 %$\Delta\rho$/%-void during SU and EOC, respectively. Additionally, the total power defect in the reactor is calculated as 0.63 %$\Delta\rho$ The NNS design is shown to be safe in terms of fuel temperature, moderator temperature and void increases.

The presence of the heavy water reflector tank prompts D_2O-H_2O mixing concerns, which requires understanding the reactivity feedback induced by mixing the two liquids in the core. Two mixing mechanisms are assessed for the NNS between the reflector tank and reactor primary. The core's reactivity decreases with increasing atomic percentage of light water in the reflector tank, with mixing reactivity coefficients of -0.245 %$\Delta\rho$/atom% and -0.214 %$\Delta\rho$/atom% at SU and EOC, respectively. An atomic percentage increase of heavy water in the primary decreases the reactivity with mixing coefficients of -0.225 %$\Delta\rho$/atom% and -0.201 %$\Delta\rho$/atom% at SU and EOC, respectively. Finally, the 2nd shutdown mechanism—the reflector dump system—analyses are performed for the NNS. The results show that if all the D_2O reflector is dumped from the reflector tank, the core experiences reactivity feedbacks of -47.6 %$\Delta\rho$ and -41.3 %$\Delta\rho$ at SU and EOC, respectively. This means that draining the reflector tank system can induce enough negative reactivity to safely shut down the NNS. All assessments demonstrate that the current iteration of the NNS core design is feasible and safe from a neutronics perspective.

5. Future work

This work highlighted the preconceptual neutronics analysis conducted to characterize the behavior of the NNS at multiple cycle states of operation. An MCNP model was developed, and preliminary spatial power-peaking distributions were obtained. Even though the obtained results demonstrate that the design is within nuclear criticality safety requirements, further studies are necessary to assess the equilibrium cycle, startup cycle behavior, and further understand reactivity feedback and kinetics parameters at different states. As mentioned, during startup, safety blades are inserted 7 cm to compensate for the initial excess reactivity. Detailed analyses is being performed to determine the first startup core loading requirements including non-fueled plates in some FA's.

With two hafnium control blades used to control the reactor and all calculation and past experience of NCNR engineers show that the reactor can be designed and operated with the blades. However, to speed up the reactor control response and compensate for the small reactivity changes, a possible regulating rod design should be considered to add to the design of the NNS.

Current neutronics analysis employed cross-section libraries found in the ENDF/B-VII.1 and ENDF/B-VIII.0 databases. However, temperature-dependent cross-section data should be generated for a high-fidelity representation of the core. Existing MCNP cross-section data libraries were generated at a limited number of temperatures, tailored for typical power reactor conditions. More detailed temperature treatment is planned for future conceptual and design phases of the NNS by generating temperature-dependent cross-sections with the NJOY [15] nuclear data processing code. Such thermal-hydraulics feedback in future analyses would require potential multiphysics coupling routines. These cross-section sets shall be verified with the ICSEP [16] data and/or experiments. Once the verification process is complete, power reactivity calculations and moderator temperature reactivity calculations shall be repeated. Temperature dependency may be relevant in the moderator temperature coefficients analysis. Thermal-hydraulics feedback for zero power and full power shall be incorporated with the neutronics in the future to enable coupled analyses that would allow an improved understanding of the reactor's criticality safety behavior.

Although all the existing analyses pass the basic statistical checks for Monte Carlo particle transport simulations, a deeper understanding of the uncertainty and sensitivity of the criticality safety behavior to variations in the design is needed. This is relevant when considering the practicality of the proposed reactor concept, where manufacturing tolerances, material impurities, and operational inconsistencies due to measurement uncertainties and noise are expected. But their impacts on the safety of the core are widely unknown at this stage of the design. Addressing this requires performing sensitivity analyses and therefore a multitude of simulations to check for variations in the design parameters (e.g., FP thickness). This can be computationally expensive, which can be offset by low-order or simplified models that retain the same fidelity of results while minimizing computational expense [17]. Such models are beneficial for parametric design and optimization studies, and they shall be pursued in the future.

Another future work is the parametrized model optimization. Model flexibility is important to optimize reactor core material and geometry, to evaluate principal component analysis for uncertainty quantification, and to assess limiting safety system settings. To perform this, an object-based core input generator could be scripted. Such a system would use standard structures in an object-based modular solution.

More detailed neutron flux profile analyses are necessary to further optimize the scientific throughput (i.e., maximizing leaked thermal neutron flux). Considering the results shown in Figure 13, the epithermal neutrons are maximized at the interface between the cold source and the core, which may enable the addition of a hot neutron source or a rabbit system for neutron activation analyses—an experimental capability that the NNS does not accommodate. Such variations in the design will alter all the criticality safety results presented in this report. So, it is beneficial to gain a deeper understanding of the energy-grouped neutron flux behavior throughout the reactor; and develop computational tools that enable quick and flexible variations in the core design while maintaining sufficient safety margins (similar to existing analysis tools used for the NBSR's alternative fuel management schemes analyses [18]). Future work shall pursue the development and verification of such tools, and it shall pursue such flexible design optimization analyses.

The CNSs are in close physical proximity to the core such that the core cannot be isolated and analyzed by itself. Core dimensions and CNS locations shall be optimized considering the cold neutron sources even when they are non-operational. Furthermore, CNS's jacket(s) filled with D_2O and beam tubes filled with D_2O (etc.) could be evaluated to optimize plant performance. Figure 12 through Figure 15 show the neutron flux distributions with multiple energy groups. Most cold neutrons are concentrated inside the CNSs at all cycle states.

Simultaneously to this report, thermal-hydraulics steady state and accident analyses are conducted to ensure the overall safety of the reactor and its systems [19]. Thermal-hydraulic coupling effects are an ongoing work subject, which allows an understanding of the the thermal safety's sensitivity to neutronics model-related phenomena, such as the number of particles in the Monte Carlo model.

References

[1] Werner CJ, Brown FB, Bull JS, Casswell L, Cox LJ, Dixon DA, Forster RA, Goorley JT, Hughes HG, Solomon CJ, Favorite J, Martz RL, Mashnik SG, Rising ME (2017) MCNP Users' Manual Code Version 6.2. (Los Alamos National Laboratory), LA-UR-17-29981. Available at https://mcnp.lanl.gov/pdf_files/la-ur-17-29981.pdf

[2] Mosteller RD (2002) Validation suites for MCNP. (Los Alamos National Laboratory, United States), LA-UR--02-0878.

[3] Yang X, Satvat N (2012) MOCUM: A two-dimensional method of characteristics code based on constructive solid geometry and unstructured meshing for general geometries. *Annals of Nuclear Energy* 46:20–28.

[4] Arsenault B, Shaikh O, Downar T, Jabaay D, Ward A, Xu Y (2015) Benchmarking of a generic CANDU reactor with PARCS, MCNP and RFSP, US NRC. (NUREG/IA-0453).

[5] Nuclear Regulatory Commission, Washington, DC (United States). Office of Nuclear Reactor Regulation (1996) Guidelines for preparing and reviewing applications for the licensing of non-power reactors: Standard review plan and acceptance criteria., NUREG-1537 Pt.2, 211545. https://doi.org/10.2172/211545

[6] Robinson AB, Chang GS, Keiser J, Wachs DM, Porter DL (2009) Irradiation Performance of U-Mo Alloy Based 'Monolithic' Plate-Type Fuel – Design Selection. (Idaho National Lab. (INL), Idaho Falls, ID (United States)), INL/EXT-09-16807. https://doi.org/10.2172/968567

[7] Turkoglu DJ, Wu Z, Williams RE, Newton TH (2018) Comparison of Neutronics Performance Characteristics of the Proposed NIST Reactor with Different LEU Fuels. *Proceedings of the PHYSOR 2018* (Cancun). Available at https://tsapps.nist.gov/publication/get_pdf.cfm?pub_id=925481

[8] Nelson T, Eddy BG (2010) Foreign Research Reactor Uranium Supply Program: The Y-12 National Security Complex Process. (Belgium), 978-92-95064-10–2, p 8. Available at http://inis.iaea.org/search/search.aspx?orig_q=RN:41064167

[9] Celikten OS, Sahin D (2021) The Effects of Impurities in Down-Blending Highly Enriched Uranium on the Reactor Neutronics and Cycle Length. (ANS, Washington, DC). Available at https://www.ans.org/pubs/transactions/article-50496/

[10] Cheng L, Hanson A, Diamond D, Xu J, Rorer D, Carew J Safety Analysis Report (SAR) for License Renewal for the National Institute of Standards and Technology Reactor – NBSR 14 Appendix A. Available at https://www.nrc.gov/docs/ML0411/ML041120250.pdf

[11] Wilson E, Stevens J,(2020) Progress on U.S and International Low-Enriched Uranium Reactor Conversions. *Transactions of the American Nuclear Society - Volume 123* (AMNS), pp 311–314. https://doi.org/10.13182/T123-33604

[12] Jaluvka D, Wilson E, Jamison L, Stillman J (2020) Experiment and Design Integration for U.S. High Performance Research Reactor Low-Enriched Uranium Conversion. *Transactions of the American Nuclear Society - Volume 123* (AMNS), pp 359–362. https://doi.org/10.13182/T123-33150

[13] Jamison L, Stillman J, Kim YS, Mouche P, Jaluvka D, Mohamed W, Wilson E (2022) Review of the Technical Basis for Properties and Fuel Performance Data Used in HEU to LEU Conversion Analysis for U.S. High Performance Research Reactors. (Argonne National Laboratory), ANL/RTR/TM-17/19 Rev. 2.

[14] American Nuclear Society (2007) ANSI/ANS-15.1-2007 (R2018) - American National Standard The Development of Technical Specifications for Research Reactors. (La Grange Park, Illinois), ANSI/ANS-15.1-2007, p 24. Available at https://webstore.ansi.org/Standards/ANSI/ANSIANS152007R2018

[15] Muir DW, Boicourt RM, Kahler AC, Conlin JL, Haeck W The NJOY Nuclear Data Processing System, Version 2016.

[16] ICSBEP Handbook 2021 https://doi.org/10.1787/2ab38d35-en

[17] Weiss AG, Tsvetkov PV, Hearne J, Kimber ML, Wootan DW, McDeavitt SM (2023) A sensitivity analysis to predict the neutronics behavior of samples irradiated in the VTR rabbit system. *Annals of Nuclear Energy* 185:109708.

[18] Şahin D, Çelikten OŞ, Gurgen A, Weiss AG, Cheng L-Y, Kohut P, Lu C, Varuttamaseni A, Newton T (2023) NBSR Alternative Fuel Management Schemes Analysis Procedure. (National Institute of Standards and Technology, Gaithersburg, MD), NBSR-0018-DOC-00.

[19] Weiss AG, Gurgen A, Bures ER, Shen JS (2024) Pre-conceptual Design Activities of the NIST Neutron Source - Preliminary Thermal-hydraulics Safety Assessments.